

Theranostics

2026; 16(4): 1782-1803. doi: 10.7150/thno.122294

Research Paper

Lactylation-driven NSUN2-mediated RNA m5C modification promotes perineural invasion in pancreatic cancer

Tianhao Huang^{1, 2, 3#}, Chonghui Hu^{2#}, Huimou Chen^{4#}, Honghui Jiang^{2, 3#}, Tingting Li^{2, 5}, Qing Tian^{2, 5}, Rihua He^{2, 3}, Yuan Yuan¹, Yong Jiang^{2, 3}, Yu Zhou², Qing Lin², Zhihua Li⁴, Mingming Xiao⁷, Xuebiao Wei^{6⊠}, Rufu Chen^{1, 2, 3, 5™}, Shangyou Zheng^{1, 2™}

- Guangdong Cardiovascular Institute, Guangdong Provincial People's Hospital, Guangdong Academy of Medical Sciences, Guangzhou, Guangdong, 510080. China.
- Department of Pancreas Center, Department of General Surgery, Guangdong Provincial People's Hospital (Guangdong Academy of Medical Sciences), Southern Medical University, Guangzhou, Guangdong, 510080, China.
- Guangdong Provincial People's Hospital (Guangdong Academy of Medical Sciences), Southern Medical University, Guangzhou, Guangdong ,510080, China.
- 4. Department of Oncology, Sun Yat-sen Memorial Hospital of Sun Yat-sen University, Guangzhou, Guangdong, 510120, China.
- 5. School of medicine, South China University of Technology, Guangzhou, Guangdong, 510006, China.
- 6. Department of Geriatric Intensive Medicine, Guangdong Provincial Geriatrics Institute, Guangdong Provincial People's Hospital (Guangdong Academy of Medical Sciences), Southern Medical University, China.
- 7. Department of Pancreatic Surgery, Fudan University Shanghai Cancer Center, Shanghai 200032, China.
- # These authors contributed equally to this work.
- ⊠ Corresponding authors: Xuebiao Wei, address: Department of Geriatric Intensive Medicine, Guangdong Provincial Geriatrics Institute, Guangdong Provincial People's Hospital (Guangdong Academy of Medical Sciences), Southern Medical University, Guangzhou, 510120, China; E-mail: weixuebiao@163.com; Phone: 86020-83827812. Rufu Chen, address: Guangdong Provincial People's Hospital (Guangdong Academy of Medical Sciences), Guangzhou, 510080, China; E-mail: chenrufu@gdph.org.cn; Phone: 86020-83827812. Shangyou Zheng, address: Guangdong Provincial People's Hospital (Guangdong Academy of Medical Sciences), Guangzhou, 510080, China; E-mail: zhengshangyou@gdph.org.cn; Phone: 86020-83827812.
- © The author(s). This is an open access article distributed under the terms of the Creative Commons Attribution License (https://creativecommons.org/licenses/by/4.0/). See https://ivyspring.com/terms for full terms and conditions.

Received: 2025.07.23; Accepted: 2025.10.31; Published: 2026.01.01

Abstract

Background: Perineural invasion (PNI) is a key biological feature underpinning the high malignancy and poor prognosis of pancreatic ductal adenocarcinoma (PDAC). Lysine lactylation (Kla), a metabolite-stress-induced post-translational modification, plays crucial regulatory roles in diverse biological processes. The RNA methyltransferase NSUN2 is essential for cancer invasion and metastasis. However, the mechanisms by which NSUN2 contributes to lactylation-driven PNI in PDAC remain to be elucidated.

Methods: We assessed tumor lactate / pan-lactylation, *NSUN2* lactylation, and PNI in human PDAC cohorts with survival follow-up. Functional studies used PDAC cell lines for migration/invasion assays, dorsal-root-ganglion (DRG) co-culture, and neurite-outgrowth assays under lactate or enzymatic perturbations. Mechanistic interrogation combined *NSUN2* knockout, CRISPR knock-in mutants at K692 (K692R/E), co-immunoprecipitation, RIP-seq, MeRIP-qPCR, and actinomycin-D chase to test mRNA binding, m5C modification, and stability of *CDCP1/STC1*. *In vivo* validation employed a sciatic nerve invasion model and a KPC genetically engineered mouse model to assess tumor-nerve infiltration and disease progression.

Results: Lactylated *NSUN2* is markedly upregulated in mice and human PDAC with more severe PNI, and is significantly associated with poorer prognosis. Functionally, inhibiting lactylation or blocking *NSUN2* markedly attenuated tumor-nerve interactions and neural invasion. Mechanistically, lactate accumulation leads to the lactylation of *NSUN2* at lysine 692 (K692), subsequently inhibiting its ubiquitination and degradation. lactylation of *NSUN2* mediated m5C modification on *CDCP1* and *STC1* mRNA, enhanced their mRNA stability.

Conclusions: This study identifies lactate-driven NSUN2 K692 lactylation as a key driver of perineural invasion in PDAC. We define a lactate-NSUN2-m5C-CDCP1/STC1 axis that links metabolic stress-induced lysine lactylation to mRNA methylation-dependent stabilization of pro-invasive transcripts, highlighting actionable therapeutic targets to restrain neural invasion and improve patient outcomes.

Keywords: pancreatic ductal adenocarcinoma (PDAC), NSUN2, m5C, lactylation modification, perineural invasion

Introduction

Perineural invasion (PNI) represents a hallmark pancreatic biological feature of carcinoma, characterized by tumor cell tracking along perineural spaces of surrounding nerves, thereby promoting local dissemination and distant metastasis [1]. Clinically, PNI correlates strongly with early tumor progression, postoperative relapse, and serves as an independent predictor of unfavorable prognosis. Pancreatic ductal adenocarcinoma (PDAC) exhibits an exceptionally high prevalence of PNI, observed in approximately 80-100% of cases [2]. Early alterations in nerve architecture can already be observed at the preinvasive epithelial stage [3,4]. Our earlier randomized controlled trial (RCT) revealed that integrating modified retroperitoneal nerve dissection into standard Whipple surgery markedly enhanced disease-free survival (DFS) among patients with pancreatic head cancer. Moreover, this surgical approach effectively mitigated postoperative back pain, underscoring the pivotal role of PNI as a therapeutic target in pancreatic cancer management

RNA methylation, a form of epigenetic modification that preserves the gene sequence, is critical for regulating a wide range of biological functions. Proteins involved in this process are classified into three main groups: 'writers' that add methyl groups to RNA, 'erasers' that remove them, and 'readers' that identify and bind to these methylated RNA molecules. Although significant progress has been made in understanding the structure and pharmacology of RNA methylation regulators, the role of post-translational modifications (PTMs) in regulating these proteins has been largely overlooked. 5-Methylcytosine (m5C), a key epigenetic mark, is an RNA modification extensively found in eukaryotic ribosomal, messenger, transfer, and long non-coding RNAs. It has a vital role in regulating cellular functions by influencing RNA stability, nuclear export, translation efficiency, and processing. Accumulating evidence has revealed a complex link between m5C modification and cancer development [6-9], and our recent findings further demonstrate that cancer-associated fibroblasts (CAFs) can promote PNI in pancreatic cancer through extracellular vesicle (EV) delivery of lncRNA-PIAT, which mediates m5C modification [10]. However, the precise role of m5C modifications in lactate metabolism-driven PNI in pancreatic cancer remains to be fully elucidated.

Lactate, a byproduct of glycolysis, has been shown to contribute to tumor progression by supplying energy during tumorigenesis and facilitates immune evasion by creating an acidic microenvironment [11-13]. Beyond its established metabolic role, lactate has been identified as a key factor in generating a novel post-translational modification, lysine lactylation (Kla), which occurs on both histone and non-histone proteins [14-16]. In PDAC, Li et al. revealed lactate-dependent histone lactylation, particularly H3K18la, plays a key role in driving adenocarcinoma pancreatic ductal progression through a glycolysis-linked positive involving loop feedback mitotic checkpoint regulators, suggesting novel targets for PDAC therapy [17]. However, the effect of the novel Kla modification on the epigenetic landscape and its contribution to PNI in pancreatic cancer remains to be determined.

Our study focused on uncovering how lactate mediates neural infiltration in PDAC. Using both in vivo and in vitro systems, we observed that elevated lactate and lactylation levels markedly enhance the invasion of tumor cells towards nerves. Mechanistically, our results indicate that increased lactate induces lactylation of NSUN2 at lysine 692, thereby inhibiting its ubiquitination and subsequent degradation. This stabilization of NSUN2 leads to the upregulation of CDCP1 and STC1 mRNA via m5C-dependent mechanisms, ultimately driving PNI. These findings underscore the essential role of intracellular lactate in facilitating PNI through NSUN2 lactylation and RNA m5C modification, providing a potential therapeutic strategy to target lactylation or m5C modification in the treatment of PDAC.

Materials and Methods

Patients and specimens

From December 2014 to October 2023, a total of 142 pancreatic ductal adenocarcinoma (PDAC) specimens were obtained from patients undergoing surgical resection at Guangdong Provincial People's Hospital. Eligible participants were those with histologically confirmed PDAC who had not received any preoperative radiotherapy or chemotherapy. Individuals with a history of previous malignancies or prior cancer-related treatments were excluded from enrollment. Patients lacking complete follow-up data were also omitted from analysis. The study population included participants of both sexes, and gender balance had no influence on the inclusion of clinical samples. Each participant signed informed consent documents, experimental protocols were reviewed and approved by the Guangdong Provincial People's Hospital's Ethics Committees.

PNI is defined by the occurrence of cancer cells along nerve (cells encircle roughly one-third or more

of the neural perimeter, and / or penetrate the epineurium, perineurium, or endoneurium). The severity of PNI was determined based on both degree and frequency of PNI. The scoring for PNI degree was as: 0 (none), 1 (perineural, indicated that cancer cell encircle roughly one-third or more of the neural perimeter) and 2 (intraneural, indicated that cancer presented within epineural, perineurial, endoneurial space of the neuronal sheath). The scoring for PNI frequency was as: 0 (none), 1 (low), 2 (frequent) and 3 (excessive). The overall PNI score was calculated as the product of its extent and occurrence frequency. The severity of PNI was evaluated by final score with a cut-off point of < 4 versus ≥ 4. Patients with severe PNI (score of 4-6) were divided into 'with PNI group' (PNI+) and others (score of 0-3) were divided into 'without PNI group' (PNI-).

Multiplexed immunofluorescence

To perform multiplexed immunofluorescence, tissue sections were stained by PANO 4-plex IHC Kit (Panovue, China) following supplier's protocol. In paraffin-embedded tissue slides deparaffinized and rehydrated, followed heat-induced antigen retrieval with EDTA buffer (pH 9.0). To minimize nonspecific reactions, endogenous peroxidase activity was quenched using a blocking reagent (Golden Bridge Biotechnology, China) for 10 min, after which the sections were further blocked with goat serum (Golden Bridge Biotechnology, China) for 15 min. Subsequently, the slides were treated with primary antibodies against Tuj1 (D65A4, CST), CK19 (D4G2, CST), Pan-lac (PTM-1401RM, PTM Biolabs), NSUN2 (20854-1-AP, proteintech), STC1 (20621-1-AP, proteintech) and CDCP1 (12754-1-AP, proteintech)) for a 1 h incubation. After three washes with TBST, HRP - conjugated secondary antibodies were applied for 30 min, followed by fluorescent tyramide amplification for 15 min. Finally, nuclei were stained with DAPI, and fluorescence images were acquired with a Zeiss LSM900 confocal microscope (Carl Zeiss Microscopy).

Immunofluorescence staining

For cell, PANC-1 cells cultured on confocal dishes were first treated with 4% paraformaldehyde for fixation at room temperature and then exposed to 0.5% Triton X-100 for permeabilization. After fixation and permeabilization, blocking was performed at 37 °C for 1 h in PBS supplemented with 1% BSA and 0.1% Triton X-100 to reduce background staining. The primary antibodies, prepared in the same blocking buffer, were added to the cells and incubated overnight at 4 °C. After three washes with PBS,

dye-conjugated secondary antibodies diluted in blocking buffer were applied for 1 h away from light. Following another three PBS washes, the nuclei were counterstained with DAPI for 10 min. Fluorescence images were acquired with a Zeiss LSM900 confocal microscope (Carl Zeiss Microscopy, Germany).

Western blot analysis

Cell samples are lysed on ice for 20 min in RIPA buffer supplemented with protease and phosphatase inhibitors at a dilution of 1:1:100. The lysates were then centrifuged at 12,000 rpm for 30 min at 4 °C, and the resulting supernatant were collected. Protein concentration were quantified using a BCA Protein assay kit. Equal amounts of protein samples were separated by SDS-PAGE according to molecular weight and electrotransferred onto polyvinylidene fluoride (PVDF) membranes (Millipore, USA). The membranes were blocked with a quick blocking solution (epizyme, China) for 30 min at room temperature and subsequently incubated overnight at 4 °C with the corresponding primary antibodies. After washing with TBST buffer three times, HRP conjugated secondary antibodies were applied 1 h at room temperature. Protein bands were detected using a Chemi XT4 imaging system. The list of antibodies used in this study is provided in Table S1.

Lactate concentration measurement

After centrifugation at 12,000 × g for 10 min, the supernatant of the cell culture was collected. Lactate production was measured using a Lactate Assay Kit (Solarbio, Beijing, China) according to the manufacturer's instructions. The absorbance was recorded at 570 nm using a spectrophotometer, and lactate levels were normalized to cell number.

Neural invasion in vitro model

To evaluate cell migration and invasion, pretreated PANC-1 cells (2×10^5) were plated in 200 μ L of DMEM without serum containing or lacking 30 mM L-lactate (Sigma-Aldrich, Cat#L6402). The lower chambers contained DMEM with 10% FBS. After 10 h, non-migrated cells were carefully wiped off, and migrated cells were fixed (4% paraformaldehyde, 10 min) and stained (crystal violet, 10 min). Cell numbers were determined microscopically to evaluate cell migratory and invasive activity.

For DRG cells' neurite length analysis, pretreated tumor cells (2×10^5) were placed in the upper compartment of a 6-well Transwell apparatus containing a 0.4-µm filter membrane, and primary DRG cells (2×10^5) were placed in lower chamber. The total nerve axon length per square millimeter was recorded by phase-contrast microscopy at 6, 12, 18, 24,

30, 36, 42, and 48 h.

For the co-culture analysis of DRG and tumor cells, Panc-1 cells were resuspended in Matrigel (Invitrogen, USA) and seeded in 10 µL onto a 6-well plate. DRG explants isolated from neonatal rats were placed 3 mm away from the Panc-1 cells in 10 µL of Matrigel. After allowing the Matrigel to solidify by incubating at 37 °C for 20 min, the designated conditioned medium containing or lacking 30 mM L-lactate (Cat#L6402, Sigma-Aldrich), which was replenished every 48 h. Phase-contrast microscopy was acquired on first and seventh day of coculture with an optical imaging system (Invitrogen, USA). The neural invasion index was determined according to the following formula: 1 - (distance between the tumor front and DRG on seventh day) / (distance between the tumor front and DRG on first day).

Dorsal root ganglia (DRGs) and DRG cells isolation from neonatal Sprague-Dawley rats

After humane euthanasia of neonatal Sprague-Dawley rats, the spinal cords were quickly dissected, and DRGs were carefully collected and placed into F12 medium (Gibco, USA) for subsequent use. To obtain single DRG cells, the isolated ganglia were enzymatically dissociate at 37 °C for 30 min in a digestion buffer collagenase (Sigma-Aldrich, USA) and trypsin (Sigma-Aldrich, USA). After digestion, the resulting cell suspension was washed with DMEM supplemented with 10% fetal bovine serum and centrifuged. The collected cell pellet was resuspended in fresh medium for further analysis.

m5C dot blot assay

After treating wild-type or *NSUN2*-knockout PANC-1 cells with ddH2O or L-lactate for 2 days, total RNA was extracted and diluted uniformly to 300 ng/μL. The samples were denatured at 95 °C for 3 min and immediately cooled on ice. Then, 2 μL of the sample was spotted onto an NC Transfer Membrane (Merck Millipore, Germany) and cross-linked under UV light for 20 min. After washing the membrane with TBST buffer, it was blocked in buffer for 1 h at ambient temperature. Primary antibody (anti-m5C, 1:5000; Proteintech) was applied overnight at 4 °C, followed by secondary antibody incubation for 1 h at ambient temperature. After 5 min ECL development, chemiluminescent bands were captured using a Chemi XT4 detection unit.

qRT-PCR assay

Total RNA was isolated from cultured cells and tissue specimens using the EZB-RN4 extraction kit (EZB Bioscience). Complementary DNA (cDNA) was synthesized from purified RNA with the PrimeScript

RT Reagent Kit (Vazyme, China) according to the manufacturer's protocol. Quantitative real-time PCR was then performed using the Vazyme SYBR-based system. Relative mRNA expression levels were calculated with the 2-DACT algorithm. Primer sequences used in this study are listed in Table S1.

Immunoprecipitation assay

Cell samples are lysed on ice for 15 min using IP lysis buffer containing protease and phosphatase inhibitors, prepared at a dilution ratio of 1:1:100. The lysate is centrifuged at 13,000 g for 10 min at 4 °C. After centrifugation, the supernatant is incubated overnight at 4 °C with the target antibody or IgG antibody. Protein A/G magnetic beads (Invitrogen, USA), pre-washed with wash buffer, are added to the mixture and incubated at room temperature for 1 h. After washing the beads with wash buffer, 100 μL of elution buffer (Invitrogen, USA) is added, and the mixture is left at room temperature for 10 min. The precipitated proteins are then analyzed by Western blotting.

Mass spectrometry

Protein samples obtained from co-immunoprecipitation (CO-IP) were resolved by SDS-PAGE and visualized using Coomassie Brilliant Blue staining. The protein bands showing differential intensity were excised and submitted to APTBIO (Shanghai, China) for mass spectrometric analysis. Lyophilized peptide samples were redissolved in double-distilled water containing 0.1% formic acid, and 2 µL of each solution was injected onto a nanoViper C18 trap column (Acclaim PepMap 100, 75 µm × 2 cm). Peptide separation was performed on a nanoElute system (Bruker) with Solvent A (0.1% formic acid in 99.9% water) and Solvent B (0.1% formic acid in 99.9% acetonitrile). The samples were initially loaded in 95% solvent A and then separated on an EASY-nLC analytical column (Thermo Scientific, 15 cm \times 150 μ m, 3 μ m, C18) using a 30 min gradient at a flow rate of 300 nL/min: 5% - 35% B for 18 min, 35% - 80% B for 2 min, and 80% B for 10 min. Mass spectrometric detection was carried out on a timsTOF Pro instrument (Bruker) operated in positive ion mode. The electrospray voltage was set to 1.5 kV, and precursor as well as fragments were analyzed using a TOF mass range of m/z 100 - 1700. The timsTOF Pro was run in parallel accumulation serial fragmentation (PASEF) mode, and data were acquired using the following parameters: 1 MS scan followed by 8 MS/MS PASEF scans per cycle; total cycle time = 0.95 s; ion charge range = 0 - 5; and active exclusion enabled with a release duration of 24 s.

RNA immunoprecipitation sequencing (RIP-seq)

RIP was carried out using the EZ-Magna RIP kit (Millipore, USA). Briefly, after removing DNA from the cell lysate, immunoprecipitation is performed by incubating the lysate with the target antibody at 4 °C overnight for RNA-protein complex formation. Following this, equilibrated A/G magnetic beads are added, and the mixture is incubated at 4 °C for 1 h. Finally, RNA is extracted using the Trizol method. Finally, the precipitated RNAs were purified for deep sequencing. Purified RNA was subjected to 2 × 150 bp paired-end sequencing (PE150) on an illumina Novaseq[™] 6000 platform (LC-Bio Technology CO., Hangzhou, China) following procedures. Specifically, differential peak analysis between the experimental and control groups was performed using MAnorm. This software first merges peaks identified independently in the experimental and control IP samples, and then performs differential analysis based on the number of reads mapped to the merged peaks in each group. Differentially expressed genes (DEGs) were further identified with DESeq2, applying thresholds of Fold Change > 2 and p < 0.05.

UV cross-linking and immunoprecipitation (CLIP)

The CLIP assay was performed using the EZ-Magna RIP kit (Millipore, USA) in accordance with the manufacturer's instructions. Initially, cells were pre-treated and subjected to UV crosslinking at 254 nm with a dose of 400 mJ/cm², followed by lysis using RIP lysis buffer. The resultant lysates were then sonicated, and RNase I (Life Technologies) along with Turbo DNase (Life Technologies) was applied. Subsequently, magnetic beads, pre-coated with 1 µg of the specified antibody or anti-IgG, were introduced to the cell lysate and incubated overnight at 4 °C. The RNA precipitated from this mixture was released through treatment with proteinase K subsequently analyzed by qRT-PCR.

m5C quantification (m5 C-RIP-qPCR)

The m5C levels in indicated transcripts were measured by m5C RNA immunoprecipitation followed by qRT-PCR. Briefly, total RNA is extracted from specified cells and purified into mRNA using the Dynabeads mRNA Purification Kit (Ambion, USA). The mRNA fragments are incubated overnight at 4 °C with an anti-m5C antibody (ab10805, Abcam) or control IgG antibody, followed by a 2 h incubation with Protein A/G magnetic beads at 4 °C. After three washes, RNA is purified using the Trizol method, then analyzed by qRT-PCR. Ten percent of the mRNA

fragments are used as input, with primers listed in Table S1.

RNA stability assay

For RNA stability analysis, the indicated cells were incubated with 5 μ g/mL actinomycin D and harvested at the indicated time points (0, 3, 6, 9 and 12h). Total RNA was extracted and isolated and quantified by qRT-PCR. The mRNA half-life was determined by fitting the decay curve using a non-linear regression model (one phase decay) in GraphPad Prism.

Animal experiments

To establish the sciatic nerve invasion model, PANC-1 cells were preincubated with 30 mM L-lactate for 48 hours and transfected with shRNA against NSUN2 or a non-targeting control (shNC). BALB/c nude mice (4 weeks old, n = 15) were anesthetized and positioned prone to allow surgical access to the sciatic nerves. A total of 2 µL of tumor cell suspension (1×10^4 cells/ μ L) was injected into the right sciatic nerve using a Hamilton syringe, and as a negative control, the left sciatic nerve received an injection of the same volume of PBS. Sciatic nerve function was monitored weekly, which was defined on a 1-4 scale: A score of 4 indicated normal hind-limb motor function with full toe and ankle extension and symmetric gait, 3 indicated mild impairment with slight weakness or reduced toe spreading, 2 represented moderate dysfunction with partial foot drop and reduced voluntary movement, and 1 denoted complete paralysis with loss of voluntary motion and no measurable muscle contraction upon stimulation. To quantitatively assess paralysis severity, two complementary metrics were employed: hind-limb muscle strength was measured using a grip-strength meter. Every two weeks, the hindpaw toe-spread (first-fifth digits) was recorded to assesse the sciatic nerve index of mice. After 6 weeks, all mice were euthanized, and sciatic nerve and tumor specimens were collected and fixed in 4% paraformaldehyde for histological analysis.

Genetically engineered mouse model

Genetically engineered KPC mice (LSL-KRAS G12D/+; LSL-TP53 R172H/+; PDX-1-CRE+/+) were purchased from Shanghai Model Organisms Center. The mice were intraperitoneally injected with sodium lactate (1 g/kg, n = 15) once daily, and were injected with AAV packaging shNSUN2 (n = 15) . After a 4-week experimental period, the mice were euthanized, and pancreatic tissues were harvested, fixed in 4% paraformaldehyde, and embedded for histological analysis.

Immunohistochemistry

Paraffin-embedded tissue sections deparaffinized and rehydrated, followed by antigen retrieval in EDTA buffer for 21 min. The sections were then incubated at room temperature with a peroxide block for 10 min. Subsequently, the tissue sections were incubated overnight at 4 °C with the primary antibody against NSUN2, pan-lac, CDCP1 or STC1. Afterward, signal enhancement solution polymer-conjugated HRP-labeled goat anti-mouse/ rabbit IgG were applied and incubated at 37 °C for 20 min. The antigen location was visualized using DAB substrate, and counterstaining with hematoxylin was performed for contrast.

Plasmid construction, RNA interference, lentiviral transduction, and CRISPR-Cas9 editing

All plasmids and siRNAs used in this study were synthesized by IGE Biotechnology (Guangzhou, China), and lentiviral and CRISPR-Cas9 systems were provided by Genecefe Biotechnology (Jiangsu, China). For plasmid construction, full-length human NSUN2 and its lysine-to-arginine variants (K692R, K441R, K640R, K712R, K257R) were inserted into the pcDNA3.1 expression vector. Full-length human NSUN2 was also subcloned into a FLAG-tagged expression plasmid, while full-length Ubiquitin and GFP were ligated into an HA-tagged vectors. CRISPR-Cas9 technology was applied to establish stable NSUN2 knockout cell lines. methylation-domain mutants, and lysine-substituted variants (K692R, K692E, K692A, and K692Q). Short hairpin RNAs (shRNAs) targeting NSUN2 were designed in the pCDH-CMV-MCS-EF1-Puro backbone (sequences listed in Table S1). Plasmids transfections were carried out using Lipofectamine 3000 and P3000 reagents (Invitrogen, USA). For siRNA-mediated silencing, Lipofectamine 3000 was employed to knock down LDHA, LDHB, and NSUN2 (see Table S1 for sequences). Lentiviral-mediated gene delivery was performed following the provider's protocol, and resistant cells were maintained under puromycin pressure (A3740, APExBIO, USA) for two weeks to generate stable populations.

Generation of NSUN2 point-mutant PANC-1 cell lines

CRISPR-Cas9 ribonucleoprotein (RNP)-mediated homology-directed repair (HDR) with single-stranded oligodeoxynucleotide (ssODN) donors was employed to introduce K692E, K692R, K692Q, and K692A substitutions at the endogenous *NSUN2* locus. The DepMap database was consulted to ensure that the selected cell line harbored an

NSUN2 copy-number state suitable for genome editing. Three sgRNAs targeting the vicinity of K692 were designed and computationally screened for onand off-target efficiency. Cas9 protein and sgRNA were preassembled into RNP complexes, combined with the corresponding ssODN donor, and delivered into PANC-1 cells via electroporation. After 48-72 h, single-cell cloning was performed, and colonies were expanded in 96-well plates. Genomic DNA was extracted and PCR-amplified using primers flanking the target exon. Positive clones were initially screened by allele-specific PCR and/or restriction fragment length polymorphism (RFLP) analysis, followed by Sanger sequencing to confirm precise substitutions, zygosity, and silent mutations introduced for PAM disruption. Verified homozygous clones were expanded and subjected to quality control prior to downstream experiments. All sgRNA and ssODN sequences used in this study are listed in Table S1.

Statistical analysis

All data were performed by SPSS software (version 27.0) and GraphPad Prism (version 9.0). Quantitative results were presented as mean ± standard deviation (SD) from at least three independent experiments unless stated otherwise. Differences between two groups were assessed using either Student's t-test or the non-parametric Mann-Whitney U test according to the data distribution. For comparisons among multiple groups, one-way or two-way analysis of variance (ANOVA) was used, followed by Tukey's multiple comparison test to evaluate intergroup differences. Non-parametric categorical variables were examined by Chi-square or Fisher's exact test. The correlation between continuous variables was evaluated using Spearman's rank correlation analysis. Cox model analysis provided likelihood-ratio-based p values, and Kaplan-Meier survival plots were created with the 'survival' package to display overall survival Associations among tissue concentration, NSUN2, pan-lactylation, CDCP1, STC1 expression, and clinical outcomes (overall survival, OS; disease-free survival, DFS) were analyzed by applying a multivariate Cox proportional-hazards model, and p values below 0.05 were interpreted as statistically significant.

Ethics statement

All experimental procedures involving human tissues and animals were reviewed and approved by the Ethics Committee of Guangdong Provincial People's Hospital (approval number: KY2024-999-01). The study protocol was conducted in accordance with the principles of the Declaration of Helsinki and

relevant national regulations. Written informed consent was waived as per approved protocol version (V1.0, dated May 1, 2024). Animal studies were conducted following institutional guidelines, and the animal experiment protocol (V1.0, dated July 17, 2023) was approved by the committee.

Results

Elevated lactate and lactylation levels are associated with poor prognosis and PNI in PDAC

To elucidate the role of lactylation in perineural invasion (PNI), we assessed global lactylation in tumors from patients with and without severe PNI. Immunofluorescence analysis demonstrated that patients with severe PNI exhibited markedly elevated levels of overall lactylation compared with those without (Figure 1A-B). Moreover, elevated global lactylation levels were associated with poorer overall survival (OS) and disease-free survival (DFS) (Figure 1C-D). Given that lactate serves as a substrate for lactylation, we next examined its effect on lactylation in PANC-1 cells. Western blot analysis showed that lactylation levels increased concentration-dependent manner, peaking at 30 mM L-lactate and declining at higher concentrations (Figure 1E, Figure S1A). Functionally, 30 mM L-lactate significantly enhanced the invasive and migratory abilities of PANC-1 cells and promoted neurite outgrowth in neuronal cells (Figure S1B-C). Consistently, Dorsal root ganglia (DRG) assays showed that 30 mM L-lactate markedly promoted tumor cell invasion into the DRG and facilitated neurite extension (Figure S1D). Lactate treatment also significantly increased intracellular lactate and global lactylation levels (Figure 1F, Figure S1E). Supporting these findings, primary tumor cells isolated from patients with severe PNI exhibited higher global lactylation than those from patients without PNI (Figure S1F), and displayed greater invasive and properties well migratory as as neurite-promoting activity (Figure S1G-H). DRG assays further confirmed that primary tumor cells from patients with severe PNI showed enhanced invasion into DRG and induction of neurite outgrowth compared with cells from patients without severe PNI (Figure S1I).

To assess whether inhibiting lactylation could suppress neural invasion in pancreatic cancer, we decreased global lactylation in PANC-1 cells by transfecting siRNAs targeting *LDHA* and *LDHB*. Western blot analysis showed that knockdown of *LDHA* and *LDHB* effectively reduced global

lactvlation levels (Figure 1G, Figure S1I). Supplementation with L-lactate restored lactylation levels in LDHA/B-deficient PANC-1 cells (Figure 1G, Figure S1J). Functional assays demonstrated that LDHA/B knockdown significantly reduced the invasive and migratory abilities of PANC-1 cells, as well as neurite outgrowth in neuronal cells. Consistently, DRG assays revealed that LDHA/B knockdown markedly impaired the cells' ability to invade DRG and promote neurite outgrowth (Figure S2A-F). Notably, these effects were reversed by L-lactate supplementation (Figure 1H-M). To exclude the possibility that these phenotypic changes were attributable to altered cell proliferation, we compared colony formation and CCK-8 assays between control and lactate-treated cells under identical conditions, and found no significant differences (Figure S2G-H), indicating that the enhanced invasive behavior was not due to changes in cell growth. Collectively, these results indicated that lactylation play a critical role in PNI of pancreatic cancer.

Lactate upregulates m5C and NSUN2 levels to promote PNI in PDAC

m5C modification is implicated in a broad spectrum of biological functions [18]. Our previous studies revealed that patients with severe PNI showed a marked increase in total m⁵C levels compared with those without PNI, thereby contributing to the progression of pancreatic cancer-associated PNI [10]. However, the relationship between m5C modification and lactylation remained unclear. Intriguingly, we found that that L-lactate treatment markedly increased global m5C levels in PANC-1 cells (Figure 2A). Given that multiple RNA methyltransferases contribute to m5C modification, we assessed the expression of a panel of enzymes in response to lactate. At the mRNA level, none of these enzymes exhibited significant alterations following lactate treatment (Figure 2B). Notably, lactate treatment significantly upregulated NSUN2 protein levels, whereas the expression of the other enzymes remained unaffected (Figure 2C, Figure S3A). Consistently, immunofluorescence staining of patient samples showed that NSUN2 expression was markedly higher in tumors with severe PNI than in those without (Figure 2D). Furthermore, correlation analysis confirmed a positive association between lactylation levels and NSUN2 expression (Figure 2E). Importantly, Kaplan-Meier survival analysis demonstrated that patients with high NSUN2 expression had significantly poorer overall survival and disease-free survival compared with those with low NSUN2 expression (Figure 2F-G).

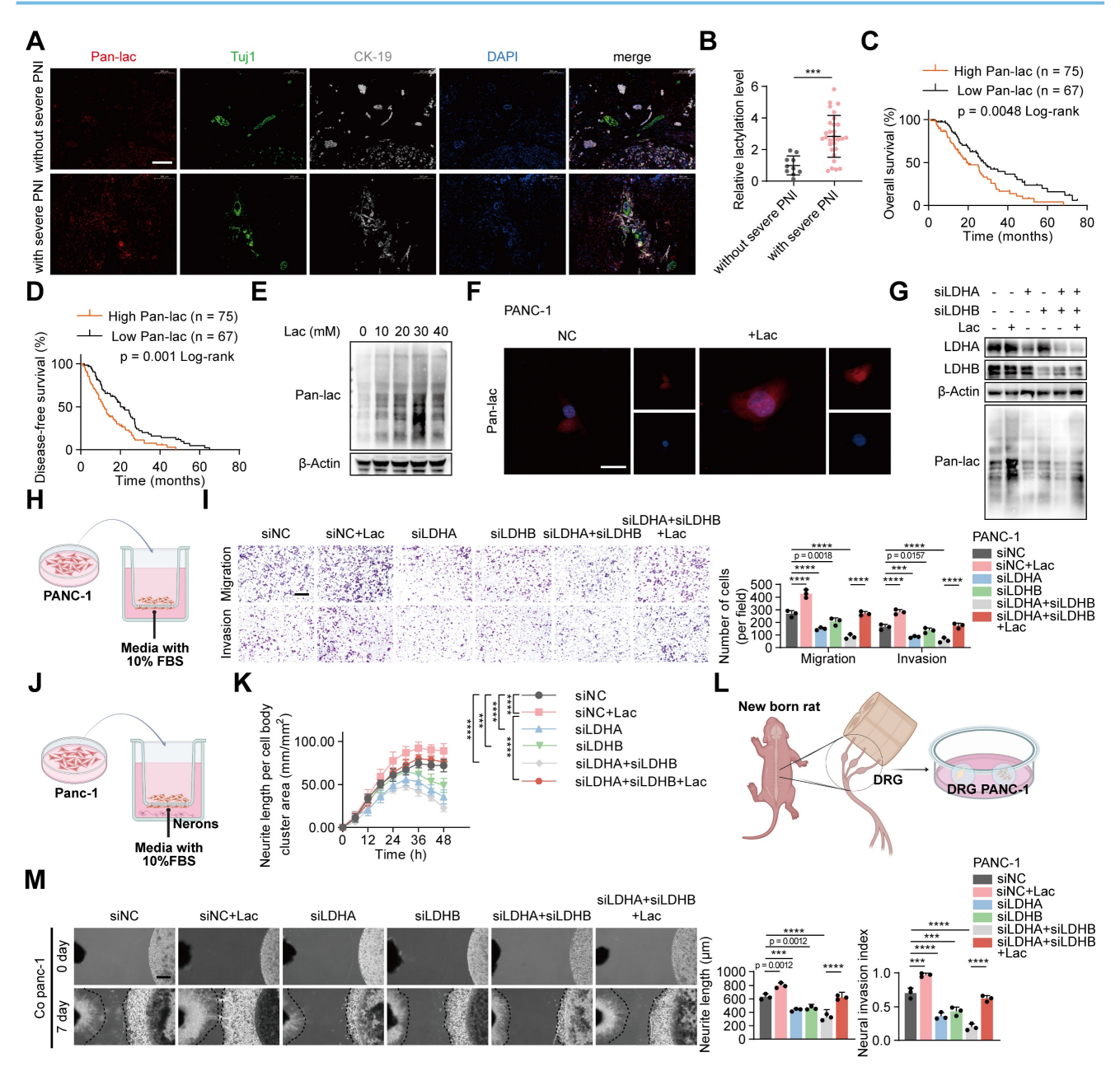


Figure 1. Elevated lactate and lactylation levels are associated with poor prognosis and PNI in PDAC. (A) Representative mIF staining for Pan-lac, *Tuj1* and *CK-19* expression in PDAC tissues grouped by PNI severity. Pan-lac reports lactylation; *Tuj1* labels neurons; *CK-19* identifies epithelial cancer cells. Scale bars, 200 μm. (B) Quantification of tissue lactylation levels in PDAC cases with or without severe PNI. (C-D) Kaplan-Meier survival curves showing OS (C) and DFS (D) in the PDAC cohort stratified by Pan-lac level (high vs low). (E) Immunoblot analysis of lactylation modification levels in PANC-1 cells following treatment with varying concentrations of L-lactate. (F) Immunofluorescence detection of Pan-lac in tumor cells treated as indicated. Scale bar, 20 μm. (G) PANC-1 cells subjected to *LDHA/LDHB* knockdown and L-lactate exposure were analyzed by Western blot to determine lactylation levels. (H-M) PANC-1 cells expressing siNC, *LDHA* siRNA, *LDHB* siRNA, or expressing both *LDHA* and *LDHB* siRNAs, followed by ± L-lactate treatment for subsequent experiments. (H) Schematic diagram of tumor cells in a Transwell assay. (I) PANC-1 Transwell migration/invasion: image panels (left) and measurements (right). Scale bar, 200 μm. (n = 3; one-way ANOVA; mean ± SD). (J) Schematic representation of the neuronal-tumor Transwell co-culture system. (K) Quantitative analysis of neurite outgrowth under the indicated conditions in the Transwell co-culture model. Phase-contrast images were obtained at 6 h intervals. (n = 3; two-way ANOVA; mean ± SD). (L) Schematic representation of the direct co-culture model between tumor cells and dorsal root ganglia (DRG). (M) (top) Representative fields from DRG co-cultures with tumor cells. (bottom) Summary statistics for tumor neurite invasion toward DRG. The black dashed line on the left indicates the growth boundary of the DRG, which on the right marks the growth boundary of PANC-1 cells. Scale bar, 500 μm. (n = 3; one-way ANOVA test; mean ± SD). **** **P < 0.0001**, ***

To further assess the role of *NSUN2* in PNI, we manipulated its expression in PANC-1 cells. Transwell and neurite outgrowth assays showed that *NSUN2* overexpression enhanced PANC-1 cell invasion and migration, as well as neurite extension in neuronal cells. DRG assays further confirmed that

NSUN2 overexpression promoted PANC-1 cell invasion into DRG and facilitated neurite outgrowth (Figure 2H-J). Conversely, NSUN2 depletion or treatment with an NSUN2 small-molecule inhibitor suppressed PANC-1 cell invasion and migration, reduced neurite outgrowth in neuronal cells, and

diminished the capacity of tumor cells to invade DRG and promote neurite extension. (Figure S3B-D). Notably, these effects were partially reversed rescued by L-lactate supplementation (Figure S3E-G). To further validate these findings, we generated an *NSUN2* knockout PANC-1 cell line. Under *NSUN2* knockout, the partial phenotypic rescue by L-lactate observed in *NSUN2*-depletion cells was largely abolished (Figure 2K-M). Importantly, re-expression of wild-type *NSUN2* in lactate-treated *NSUN2*-KO

cells restored global m5C levels and re-established the perineural invasion phenotype (Figure S3H-K). By contrast, exogenous L-lactate increased global protein lactylation irrespective of NSUN2 status, indicating that NSUN2 lactvlation represents a PNI-specific regulatory mechanism rather than a general effect on pan-lactylation (Figure S3L). These findings underscore role of the critical NSUN2 lactate-mediated PNI.

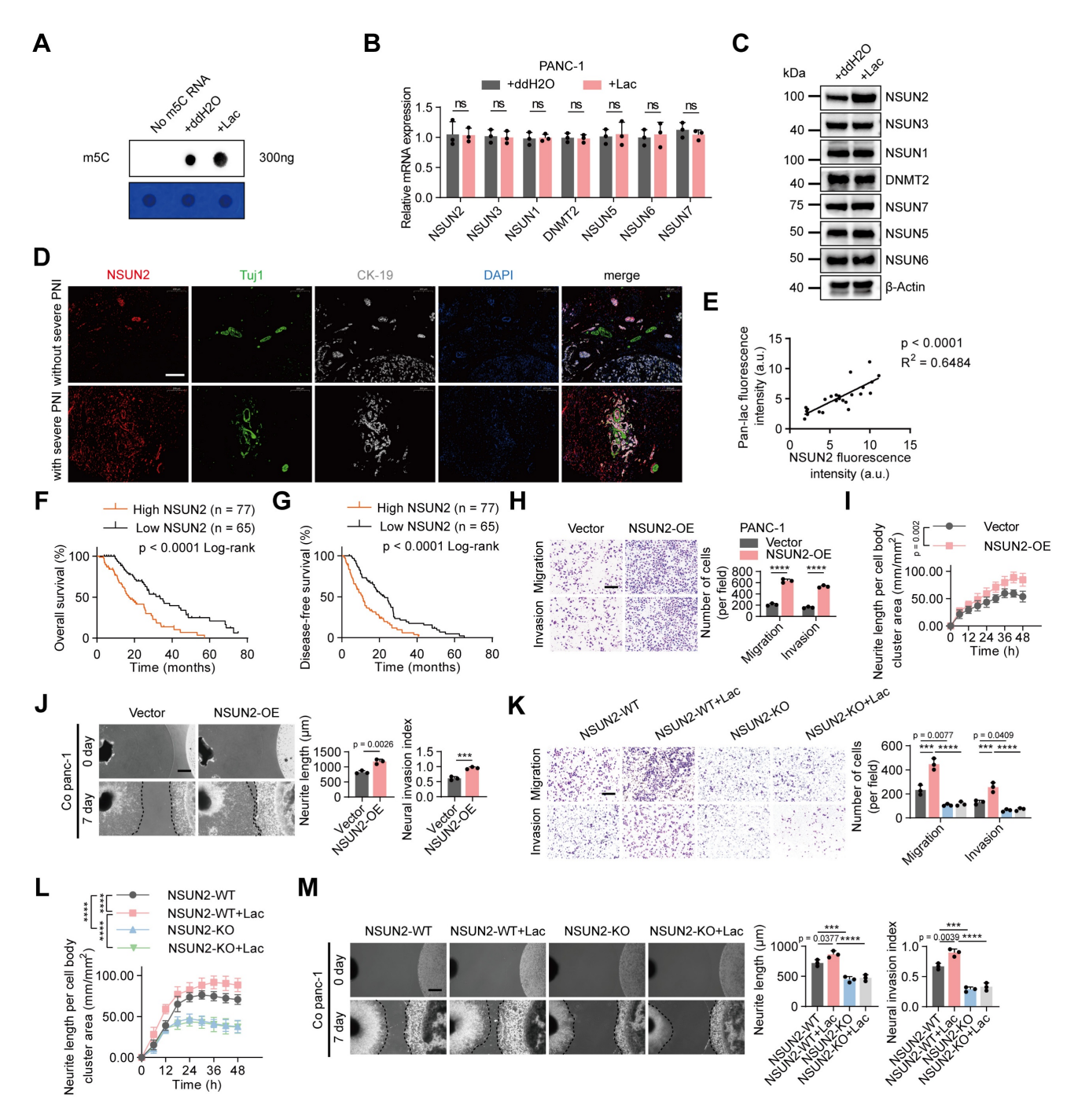


Figure 2. Lactate upregulates m5C and NSUN2 levels to promote PNI in PDAC. (A) Dot blot analysis showing m5C modification levels in total RNA isolated from PANC-1 cells treated with or without L-lactate. Methylene blue staining (below) indicates RNA loading, whereas the dot blot signal intensity (above) reflects the global m5C content. (B) Quantitative RT-PCR analysis of NSUN1, NSUN2, NSUN3, NSUN5, NSUN6, NSUN7 and DNMT2 mRNA expression levels in PANC-1 cells followed by ± L-lactate

treatment. **(C)** Immunoblot analysis of *NSUN1*, *NSUN2*, *NSUN3*, *NSUN3*, *NSUN5*, *NSUN6*, *NSUN7* and *DNMT2* protein expression levels in PANC-1 cells under the same treatment conditions. **(D)** Representative mIF staining for *NSUN2*, *Tuj1* and *CK-19* grouped by PNI severity in PDAC tissues. *Tuj1* marks neuronal cells, and *CK-19* identifies tumor epithelial cells. Scale bars, 200 µm. **(E)** Correlation between *NSUN2* expression levels and lactylation modification in 24 cases of PDAC tissues. Pearson correlation analysis was applied to estimate the coefficient (R) and significance level (P). **(F-G)** Kaplan-Meier survival curves showing OS **(F)** and DFS **(G)** in the PDAC cohort stratified by *NSUN2* level (high to estimate the coefficient (R) and significance level (P). **(F-G)** Kaplan-Meier survival curves showing OS **(F)** and DFS **(G)** in the PDAC cohort stratified by *NSUN2* level (high to estimate the coefficient (R) and significance level (P). **(F-G)** Kaplan-Meier survival curves showing OS **(F)** and DFS **(G)** in the PDAC cohort stratified by *NSUN2* level (high to estimate the coefficient (R) and significance level (P). **(F-G)** Kaplan-Meier survival curves showing OS **(F)** and DFS **(G)** in the PDAC cohort stratified by *NSUN2* level (high to estimate the control vector or *NSUN2*-OE plasmid. **(H)** Transwell-based migration/invasion: image panels (left) and measurements (right). Scale bar, 200 µm. (n = 3; unpaired t test; mean ± SD). **(J)** (left) Representative fields from DRG co-culture with tumor cells. (right) and measurements. Wild-type or *NSUN2*-knockout PANC-1 cells grouped by L-lactate treatment (with / without). **(K)** Transwell-based migration/invasion: image panels (left) and measurements. Wild-type or *NSUN2*-knockout PANC-1 cells grouped by L-lactate treatment (with / without). **(K)** Transwell-based migration/invasion: image panels (left) and measurements (right). Scale bar, 200 µm. (n = 3; one-way ANOVA test; mean ± SD). **(M)** (left) Representative flowed from DRG co-cultures with tumor

Lactylation of NSUN2 inhibits its ubiquitination and degradation

To test whether lactate regulates NSUN2 stability, cycloheximide chase assays showed that exogenous L-lactate supplementation markedly prolonged the NSUN2 half-life (Figure 3A, Figure S4A). Conversely, dual LDHA/LDHB knockdown, which reduces endogenous lactate, shortened the NSUN2 half-life (Figure 3B, Figure S4B). Consistent proteasome-mediated turnover, stabilized NSUN2, whereas lysosomal blockade with NH₄Cl or 3-MA had no effect (Figure 3C-D, Figure S4C-E). We then interrogated ubiquitination directly. cells co-expressing FLAG-NSUN2 HA-ubiquitin, exogenous L-lactate reduced the levels of polyubiquitinated NSUN2 (Figure 3E). Conversely, LDHA/LDHB knockdown increased ubiquitination (Figure 3F, Figure S4F). These results suggested that lactate regulates NSUN2 stability through a post-translational mechanism, and indeed, we found that lactate induced robust lactylation of NSUN2 (Figure 3G-I, Figure S4F-H). Moreover, this modification was markedly diminished following LDHA/B knockdown (Figure 3J-L, Figure S4I-K), confirming that both exogenous and endogenous lactate drive NSUN2 lactylation. To delineate how lactate prevents NSUN2 degradation, we focused on STUB1 (STIP1 homology and U-box containing protein 1), an E3 ligase previously reported to mediate NSUN2 degradation [19]. Coimmunoprecipitation (Co-IP) assays revealed that lactate disrupted the interaction between NSUN2 and STUB1 (Figure 3M, Figure S4L). To exclude potential confounding from other cellular proteins, we performed GST pulldown assays with purified proteins, which confirmed that NSUN2 directly binds to STUB1 (Figure 3N). Immunofluorescence analysis further demonstrated that lactate disrupted the nuclear colocalization of NSUN2 and STUB1 (Figure 3O). Quantitative image analysis using Manders' colocalization coefficient (tM1) (Figure 3P) and Pearson's correlation coefficient (Figure 3Q) consistently showed that lactate treatment significantly disrupted NSUN2-STUB1 colocalization. Collectively, these findings demonstrates

lactylation of *NSUN2* weakens the *NSUN2-STUB1* interaction, thereby preventing *STUB1*-mediated ubiquitination and degradation of *NSUN2*.

NSUN2 is lactylated at K692

To pinpoint the lactylation sites on NSUN2, we immunoprecipitation followed LC-MS/MS, identifying nine lysine residues modified by lactylation. Among these, four sites (K441, K640, K692, K712) appeared only after lactate treatment and were absent in controls, suggesting that they are modifications potential lactate-inducible with functional relevance (Figure 4A-B). To determine their importance, generated lysine-to-arginine substitutions at these four candidate sites, together with K257 as a nonresponsive control. Anti-Flag immunoprecipitation confirmed site-specific lactylation at K692 (Figure 4C). To further examine the functional relevance of this site, we compared K692 mutants with additional substitutions at K257, K441, K640, and K712. Migration, neurite outgrowth, and DRG co-culture assays revealed that mutations at K257, K441, K640, and K712 had minimal impact, whereas the K692R mutation markedly impaired these phenotypes (Figure S5A-C). This functional distinction was supported by LC-MS/MS analysis, which provided direct b-y ion evidence for lactylation at K692 (Figure 4D, Figure S5D-G). Substitution of K692 with non-lactylatable residues (K692R or K692A) enhanced NSUN2 ubiquitination and reduced its protein abundance, whereas mimicking lactylation (K692E or K692Q) suppressed ubiquitination and stabilized NSUN2 (Figure 4E-F, Figure S5H-I). We next examined how K692 lactylation influences the interaction between NSUN2 and STUB1. Using CRISPR/Cas9-engineered PANC-1 cells carrying NSUN2-K692 mutants, co-immunoprecipitation assays showed that the K692E mutation, which mimics constitutive lactylation, markedly weakened the association of NSUN2 with STUB1, whereas the non-lactylatable K692R mutant enhanced interaction (Figure 4G). To further confirm the binding region between NSUN2 and STUB1, GST pull-down assays were performed using recombinant NSUN2 fragments (aa 1-250, 251-500, and 501-767). As

expected, STUB1 specifically bound to the C-terminal fragment GST-NSUN2 (aa 501-767), but not to other regions or GST alone (Figure 4H). To further dissect the structural basis, molecular docking analyses revealed that K692 lactylation induces conformational changes that generate steric hindrance and alter electrostatic interactions at the NSUN2-STUB1 interface, thereby impairing their binding (Figure 4I). Transwell and neurite outgrowth assavs non-lactylatable demonstrated that mutants (K692R/A) significantly impaired tumor

migration/invasion and reduced neurite outgrowth activity, whereas lactylation-mimetic mutants (K692E/Q) enhanced these phenotypes (Figure 4J-K; Figure S5J-K). Consistent with these findings, DRG assays corroborated that K692 lactylation promotes the perineural invasive behavior of pancreatic cancer cells (Figure 4L; Figure S5L). Together, these results identify K692 as the critical lactylation site on *NSUN2* that inhibits its ubiquitination, stabilizes the protein, and drives PNI in pancreatic cancer.

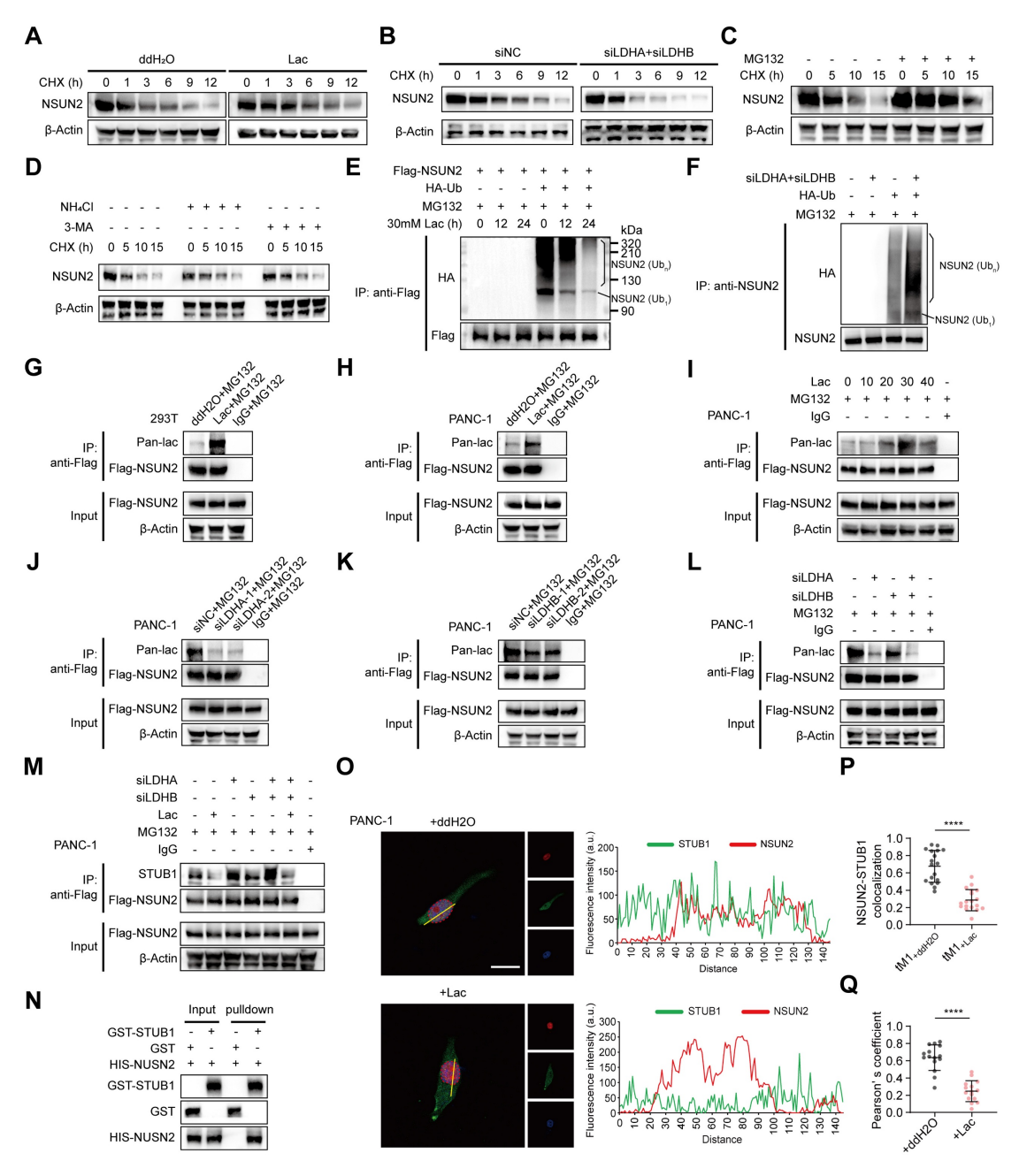


Figure 3. Lactylation of NSUN2 inhibits its ubiquitination and degradation. (A) Immunoblot analysis of NSUN2 in tumor cells exposed to ddH2O or L-lactate treatment, followed by treatment with cycloheximide (CHX) for specified time points. (B) Immunoblot analysis of NSUN2 expression in PANC-I cells carrying siNC or LDHA/LDHB siRNAs, followed by treatment with CHX for specified time points. (C) Immunoblot analysis of NSUN2 in tumor cells exposed to MG132 treatment, followed by treatment with CHX for specified time points. (D) Immunoblot analysis of NSUN2 in tumor cells exposed to NH4CI or 3-MA treatment, followed by treatment with CHX for specified time points. (E) Following plasmid transfection, PANC-I cells received MG132/L-lactate treatment for the specified intervals. Anti-FLAG immunoprecipitation of

SDS-treated whole-cell lysates was performed, and NSUN2 ubiquitination was evaluated by immunoblotting. The line labeled 'NSUN2 (Ub1)' indicates mono-ubiquitinated NSUN2, while the bracket labeled 'NSUN2 (Ubn)' marks high molecular weight polyubiquitinated NSUN2 species. (F) PANC-1 cells expressing indicated plasmids and LDHA/LDHB siRNAs were treated with MG132. Anti-FLAG immunoprecipitation of SDS-treated whole-cell lysates was performed, and NSUN2 ubiquitination was evaluated by immunoblotting. (G-H) Lactylation of NSUN2 in 293T cells (G) or PANC-I cells (H) was confirmed using an immunoprecipitation (IP) assay. 293T cells or PANC-I cells expressing FLAG-tagged NSUN2 and were exposed to ddH2O or L-lactate treatment, with concurrent treatment with MGI32. After lysis, SDS-treated extracts were subjected to anti-FLAG IP, followed by immunoblot detection. (I) Lactylation modification levels of NSUN2 in PANC-1 cells following treatment with varying concentrations of L-lactate was confirmed using an immunoprecipitation (IP) assay. (J-M) Confirmation of NSUN2 lactylation in PANC-1 cells expressing specific siRNAs by immunoprecipitation (IP). PANC-1 cells expressing FLAG-tagged NSUN2 were treated with either ddH2O or L-lactate, followed by treatment with MGI32. The cells were lysed for SDS pre-treated immunoprecipitation with anti-FLAG antibody followed by western blotting. (J) Lactylation of NSUN2 in tumor cells expressing siNC or LDHA siRNA was confirmed through immunoprecipitation (IP) assay. (K) NSUN2 lactylation in PANC-1 cells expressing siNC or LDHB siRNA was confirmed through immunoprecipitation (IP) assay. (L) NSUN2 lactylation in PANC-I cells expressing siNC, LDHA siRNA, LDHB siRNA, or both LDHA and LDHB siRNAs by immunoprecipitation (IP). (M) An immunoprecipitation blot showing the interaction levels between NSUN2 and STUB1 in PANC-1 cells transfected with siNC, LDHA siRNA, LDHB siRNA, or both LDHA and LDHB siRNAs and treated with ddH2O or L-lactate, using NSUN2 antibody in vitro. (N) GST pull-down assay showing the interaction between STUB1 and NSUN2. (O) (Left) Immunofluorescence detection of NSUN2 and STUB1 in tumor cells treated as indicated. (Right) Colocalization analysis of NSUN2 and STUB1 in the nuclei of PANC-1 cells under the same treatment conditions. The intensity profiles corresponding to the regions of interest (ROI, indicated by yellow lines) are shown. Red curve: NSUN2 relative fluorescence intensity; green curve: STUBI relative fluorescence intensity. The overlap of the red and green curves indicates the colocalization of NSUN2 and STUB1. Higher peak intensities correspond to greater levels of fluorescence expression. Scale bar, 20 μm. (P-Q) Manders' overlap coefficient (tMI) (P) and Pearson's correlation coefficient (Q) analysis of NSUN2-STUB1 colocalization in tumor cells treated as indicated. (n = 15; unpaired t test; mean ± SD). *****P < 0.0001.

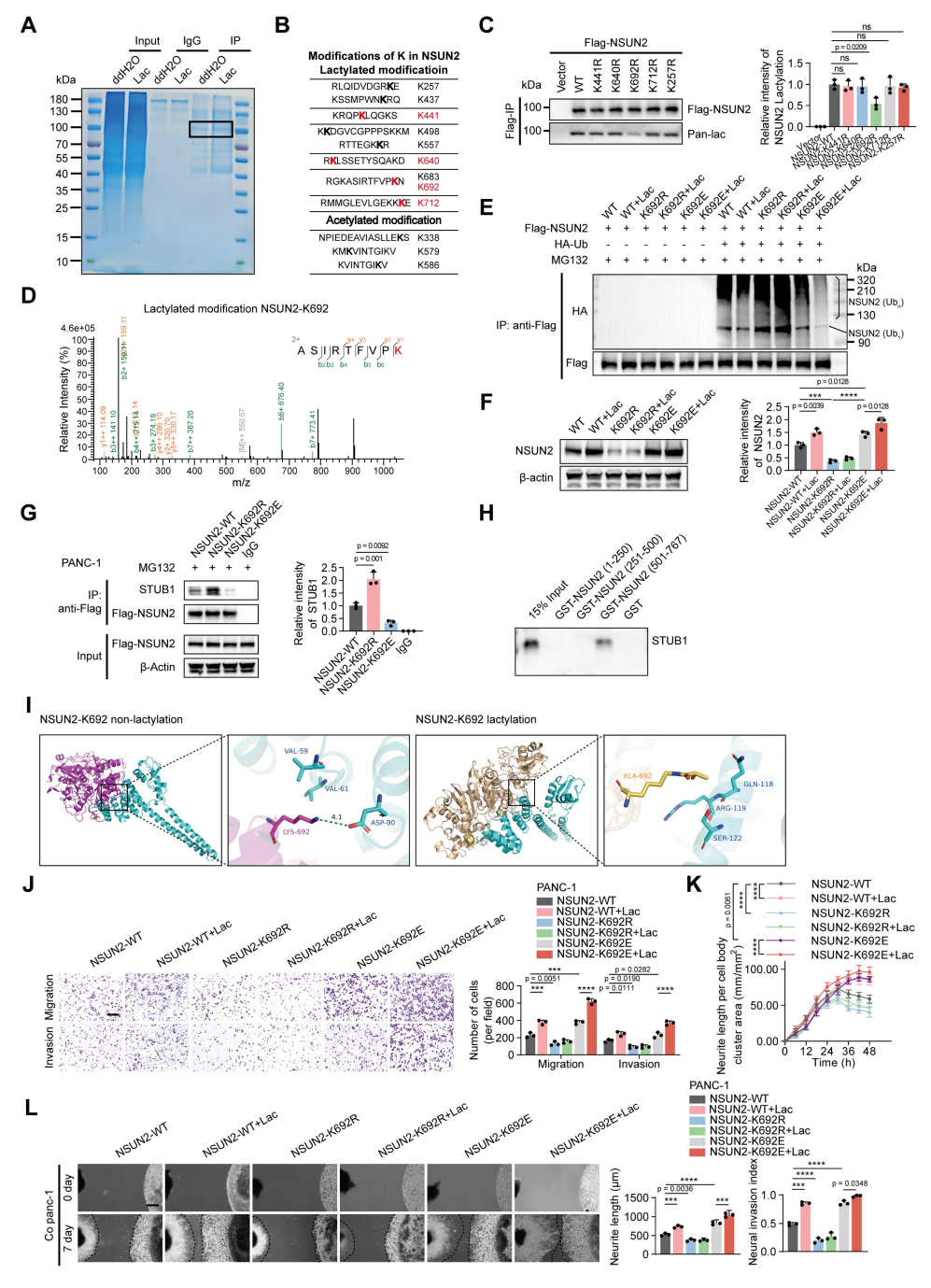


Figure 4. NSUN2 is lactylated at K692. (A) Representative Coomassie Brilliant Blue staining image of NSUN2 protein from treated tumor cells. The boxed area marks NSUN2-specific bands analyzed by LC-MS. (B) Potential modifications of lysine (K) residues in NSUN2 were assessed by mass spectrometry. Putative lactylation sites (upper

panel) and acetylation sites (lower panel) are depicted. (C) (Left) PANC-I cells were transfected with indicated NSUN2 site mutations, followed by immunoprecipitation and and Western blotting to visualize NSUN2 lactylation with pan-lactyl and FLAG antibodies. (Right) Quantification of NSUN2 lactylation intensity normalized to Flag-NSUN2 (n = 3; mean ± SD; one-way ANOVA test). (D) Mass spectra for NSUN2 peptides lactylated at K692. (E-G) NSUN2-K692 mutant PANC-I cells were generated using the CRISPR/Cas9 approach, followed by treatment with or without L-lactate and were used for the subsequent experiments. Residue K692 was replaced by arginine (K692R) or glutamine (K692E). (E) Lysates from treated PANC-I cells were SDS-pretreated, immunoprecipitated with anti-FLAG, and probed for NSUN2 ubiquitination by Western blot. The line labeled 'NSUN2 (Ub1)' indicates mono-ubiquitinated NSUN2, while the bracket labeled 'NSUN2 (Ubn)' marks high molecular weight polyubiquitinated NSUN2 species. (F) (Left) Whole-cell lysates made from PANC-I cells under the indicated treatments were used for immunoblot to assess NSUN2 protein expression. (Right) Quantification of NSUN2 intensity normalized to β-actin (n = 3; mean ± SD; one-way ANOVA test). (G) (Left) Co-IP immunoblot tillustrating the binding of STUB1 to NSUN2 in PANC-I cells with various NSUN2-K692 mutations. (Right) Quantification of STUB1 relative intensity (n = 3; mean ± SD; one-way ANOVA test). (H) In vitro binding of STUB1 to various domains of NSUN2. The in vitro translated STUB1 protein was incubated with GST, GST-NSUN2 (1-250), GST-NSUN2 (251-500), or GST-NSUN2 (501-767) in GST pull-down assays. The glutathione eluates and 15% input materials were analyzed by SDS-PAGE followed by immunoblotting with anti-STUB1 antibody. (I) Molecular docking analysis of NSUN2-STUB1 interaction before and after NSUN2 K692 lactylation. (J-L) NSUN2-K692 mutant PANC-I cells were generated using the CRISPR/Cas9 approach, followed by treatment with or without L-lactate and were used for t

NSUN2 regulates CDCP1 and STC1 expression in an m5C-dependent manner

To identify the downstream targets of the NSUN2 involved in PNI, we analyzed the mRNA expression profile of PANC-1 cells treated with L-lactate compared to control cells (Figure 5A). A total of 4419 differentially expressed genes (DEGs) were identified via mRNA sequencing (Figure 5A). Furthermore, KEGG pathway analysis indicated that increased lactylation levels upregulated signaling pathways associated with tumor invasion and metastasis (Figure 5B) [20,21]. Considering that NSUN2 functions as an m5C methyltransferase capable of selectively binding m5C-modified RNA, we next performed RNA immunoprecipitation sequencing (RIP-seq) in PANC-1 cells with or without lactate treatment. Pathway enrichment analysis of NSUN2-bound transcripts similarly highlighted signaling programs related to tumor invasion and neuronal interactions (Figure 5C). We mapped the binding motifs of NSUN2-associated mRNAs (Figure 5D) and confirmed that the NSUN2 binding sites were predominantly enriched in the coding sequence (CDS) regions of mRNA transcripts, followed by the 3' UTR (Figure 5E). Integrated analysis of RNA sequencing and NSUN2 RIP-seq identified several candidate target genes (including STC1, CDCP1, FOSL1, and Serpine1) associated with tumor invasion and neuronal interactions (Figure 5F) [22-25]. We next targets. validated these M5C-RIP assays demonstrated a marked increase in m5C modification of CDCP1 and STC1 upon lactate treatment (Figure 5G). Actinomycin D chase experiments confirmed that lactate enhanced the stability of both transcripts in an NSUN2-dependent manner (Figure 5H-I). In contrast, FOSL1 and Serpine1, although identified in the integrated analysis, exhibited no detectable changes in m5C modification or mRNA stability (Figure S6A-B), suggesting they are not bona fide NSUN2-m5C

targets. To assess whether NSUN2 is required for the lactate-induced upregulation of CDCP1 and STC1, we examined their transcript and protein levels following NSUN2 knockdown with or without lactate treatment. Lactate exposure markedly increased both mRNA and protein abundance of CDCP1 and STC1, whereas silencing NSUN2 reduced their basal expression and attenuated the lactate-induced elevation (Figure 5J-K). We next asked whether CDCP1 and STC1 mediate the PNI phenotypes. Findings from Khan, T. et al. demonstrated that CDCP1 promotes the migration and invasion of tumor cells [23]. Additionally, Liu et al. revealed that STC1 activates the MAPK/ERK signaling pathway, which plays a crucial role in cell proliferation, migration, and neuronal axon growth [22]. Consistent with these findings, our experiments demonstrated that knockdown of CDCP1 or STC1 significantly reduced tumor-cell migration and invasion, as well as neurite outgrowth and DRG invasion, whereas exogenous lactate partially restored these phenotypes (Figure 5L-M; Figure S6C-E). Furthermore, cross-linking immunoprecipitation (CLIP) analysis demonstrated that lactate treatment enhanced the selective interaction between NSUN2 and CDCP1/STC1 mRNAs (Figure 5N). Furthermore, IGV peak analysis revealed that NSUN2 binding sites were predominantly enriched in the 3' UTR region, which is known to contribute to mRNA stability (Figure 5O) [26]. To directly test whether these candidate motifs mediate m5C deposition, we generated wild-type and mutant constructs of CDCP1 and STC1 (Figure 5P). MeRIP-qPCR revealed robust m5C enrichment in wild-type constructs, which was markedly reduced in the mutants (Figure 5Q-R). Consistently, actinomycin D chase assays demonstrated that wild-type conferred greater transcript stability than their mutant counterparts (Figure 5S-T).

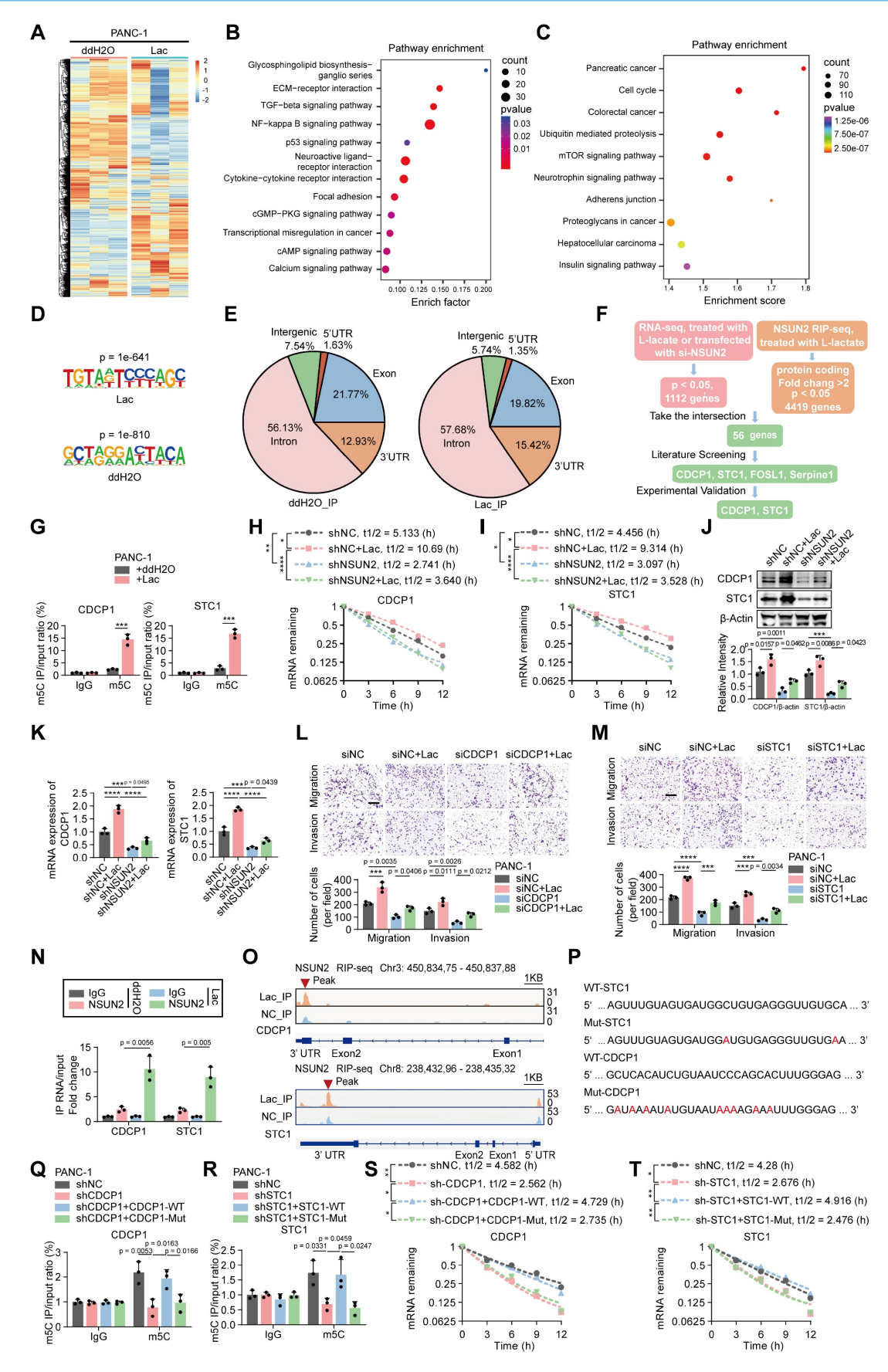


Figure 5. NSUN2 regulates CDCP1 and STC1 expression in an m5C-dependent manner. (A) Heatmap of mRNA changes in PANC-I cells exposed to ddH2O or L-lactate treatment. (B-C) Pathway enrichment mapping (KEGG) in PANC-I cells; dot size = pathway gene number, dot color = adjusted significance. (B) Pathway enrichment mapping (KEGG) of transcriptome sequencing between the control and lactate-treated groups. (C) Pathway enrichment mapping (KEGG) of NSUN2 RIP-seq between the

control and lactate-treated groups. **(D)** *NSUN2* binding Motif analysis of peak sequences using HOMER (v4.11.1) and visualization of nucleotide preferences. **(E)** *NSUN2* RIP-seq pie charts for both the ddH2O treatment (left) and L-lactate groups (right) depicting the distribution of *NSUN2* RIP-binding peaks. **(F)** Bioinformatic prediction pinpointed *CDCP1* and *STC1* as *NSUN2*-regulated genes. **(G)** MeRIP-qPCR confirmed m5C enrichment of *CDCP1* and *STC1* transcripts in PANC-1 cells ± L-lactate. **(H-I)** PANC-1 cells expressing shNC or *NSUN2*-specific shRNA, exposed to ddH2O or L-lactate treatment, were used for Actinomycin D assay to assess the half-life of *CDCP1* **(H)** and *STC1* (I) mRNA- (J-K) PANC-1 cells expressing shNC or *NSUN2*-specific shRNA, followed by specific treatment. **(J)** (Above) Immunoblot analysis of *CDCP1* and *STC1* in PANC-1 cell lysates prepared under the respective treatment conditions. (Below) Quantification of *CDCP1* and *STC1* intensity normalized to *B-actin* (n = 3; mean ± SD; one-way ANOVA test). **(K)** Total RNA isolated from treated PANC-1 cells was used for qRT-PCR analysis to assess the *CDCP1* and *STC1* mRNA expression. **(L-M)** PANC-1 cells expressing siNC, *CDCP1* siRNA **(L)** or *STC1* siRNA **(M)**, followed by treatment with or without L-lactate, were used for subsequent experiments. Transwell-based migration/invasion: image panels (top) and measurements (bottom). Scale bar, 200 µm. (n = 3; one-way ANOVA test; mean ± SD). **(N)** The interaction of *NSUN2* and the indicated mRNAs in PANC-1 cells exposed to ddH2O or L-lactate treatment was demonstrated by CLIP. **(O)** IGV tracks for *CDCP1* and *STC1* from RIP-seq analysis, peaks are marked with red triangles. **(P)** WT and potential m⁵C modification motif mutation *CDCP1/STC1* sequences were presented. Red fonts represented the mutant bases. **(Q-T)** WT-*CDCP1*, Mut-*CDCP1*, WT-*STC1* or Mut-*STC1* was overexpressed in *CDCP1/STC1* knockdown PANC-1 cells. **(Q-R)** MeRIP-qPCR analysis of *CDCP1* **(Q)** and *STC1* **(R)** mR

To further validate the regulatory axis, we examined whether NSUN2 modulates CDCP1 and STC1 expression in an m5C-dependent manner. RNA immunoprecipitation Methylated revealed that wild-type NSUN2 markedly increased m5C enrichment on CDCP1 and STC1 transcripts, whereas the catalytic mutant lost this ability (Figure S6F). Consistently, CLIP analysis demonstrated that the NSUN2 catalytic mutant exhibited markedly reduced association with both CDCP1 and STC1 transcripts (Figure S6G), accompanied by a decrease in their mRNA and protein abundance (Figure S6h-i). Decay assays further demonstrated shortened half-lives of CDCP1 and STC1 mRNAs in NSUN2-mut cells compared with NSUN2-WT (Figure S6J-K). Functionally, loss of NSUN2 catalytic activity impaired tumor-cell migration, invasion, and DRG neurite outgrowth, as shown in transwell and co-culture assays (Figure S6L-N). To further validate the regulatory role of NSUN2 lactylation in modulating CDCP1 and STC1, we assessed how K692 mutations affect their expression and stability. Compared with NSUN2-WT, the lactylation-mimetic K692E mutant markedly elevated the expression of both genes, whereas the non-lactylatable K692R mutant suppressed their expression, with lactate supplementation amplifying these trends (Figure S7A). In keeping with these findings, actinomycin D chase assays showed prolonged half-lives of CDCP1 and STC1 mRNAs in the presence of K692E, while K692R accelerated their decay (Figure S7B-C). At the signaling level, NSUN2 overexpression enhanced ERK phosphorylation and upregulated c-FOS, and these effects were abolished when STC1 was depleted or blocked by neutralizing antibody (Figure S7D). Functionally, NSUN2-driven neurite outgrowth and neural invasion were strictly dependent on STC1: silencing or antibody blockade eliminated the neurotropic advantage, whereas forced STC1 expression partially restored neural invasion under FOS knockdown conditions (Figure S7E-G). Collectively, these results demonstrate that NSUN2 regulates CDCP1 and STC1 mRNA stability in a manner dependent on m5C modification.

Impact of NSUN2 lactylation on PNI in pancreatic cancer in vivo

To evaluate the in vivo relevance of NSUN2 lactylation in perineural invasion (PNI), we employed a murine sciatic nerve invasion model. PANC-1 cells with wild-type NSUN2 or NSUN2 knockout were pretreated with either L-lactate or PBS and were inoculated into the sciatic nerves of nude mice (Figure 6A). Animals receiving NSUN2-WT cells developed progressive ipsilateral hind-limb paralysis and reduced paw span, whereas NSUN2 depletion markedly attenuated these phenotypes. Exogenous lactate exacerbated functional decline, but this effect was largely abolished in the absence of NSUN2 (Figure 6B-C). Histological and multiplex immunofluorescence analyses confirmed that NSUN2 deletion reduced tumor-induced **PNI** downregulated CDCP1 and STC1, while lactate supplementation increased pan-lactylation, NSUN2, CDCP1, and STC1 expression. Importantly, the loss of NSUN2 eliminated this lactate-driven induction (Figure 6D, Figure S8A-G).

To better mimic endogenous tumor-nerve we further utilized KPC interactions, mice (LSL-KRAS^G12D/+, LSL-TP53^R172H/+, PDX1-Cre $^+$ +) that spontaneously pancreatic cancer. In situ AAV-mediated delivery of shNSUN2 efficiently silenced NSUN2 expression, as verified by both qPCR and immunofluorescence quantification of tumor tissues (Figure S8H-J). In addition. we utilized CRISPR/Cas9-mediated frameshift mutations to achieve site-specific knockout of NSUN2 in the pancreas of KPC mice, thereby further confirming the functional role of NSUN2 in vivo (Figure 6E). One week later, mice were administered systemic lactate or PBS. Histological and multiplex immunofluorescence analyses revealed that NSUN2 knockdown suppressed CDCP1 and STC1 expression and reduced intratumoral nerve density, whereas lactate treatment partially restored these features (Figure 6E; Figure S8K-N).

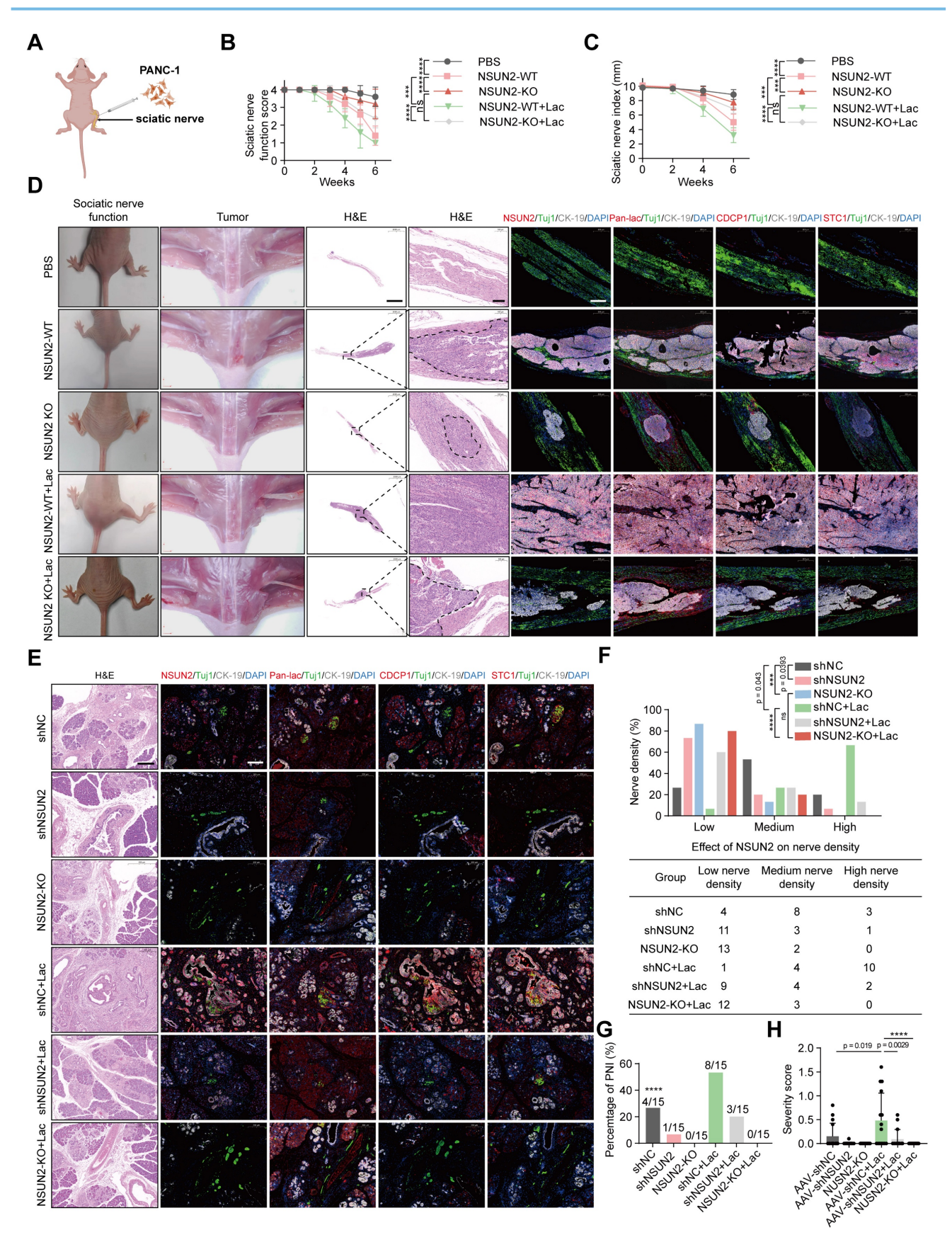


Figure 6. Impact of NSUN2 Lactylation on PNI in PDAC in vivo. (A) Schematic diagram of the sciatic nerve invasion model in nude mice. NSUN2-knockout PANC-I cells were generated using the CRISPR/Cas9 system. Wild-type or NSUN2-knockout PANC-I cells were treated with either L-lactate or PBS, followed by inoculation into the sciatic nerve of nude mice. PBS alone served as the control. (n=5 per group). (B-C) Sciatic nerve function scores (B) and sciatic nerve indexes (C) of mice treated as indicated. (n = 5; mean ± SD; Kruskal-Wallis test with Dunn's multiple comparisons test). (D) Representative gross morphology, intraoperative views, H&E and mIF images from the sciatic nerve invasion model. mIF demonstrates the expression of Pan-lac, NSUN2, CDCP1, and STC1 at the tumor-nerve interface. Dashed lines mark the tumor margins. Tuj1 serves as

a neuronal marker, whereas *CK-19* identifies tumor epithelial cells. Scale bar for H&E, 1000 μm; scale bar for mIF, 200 μm. **(E-H)** KPC mice (LSL-KRASG12D/+; LSL-TP53R172H/+; PDX-1-CRE+/+) were divided into six groups, each receiving orthotopic injections into the pancreas. Two groups were injected with adeno-associated virus (AAV) packaging short hairpin RNA negative control (shNC), while the other two groups were injected with AAV packaging sh*NSUN2*. One week later, control and experimental mice received sodium lactate (1 g/kg) or PBS intraperitoneally, respectively. n = 15. **(E)** H&E and mIF images demonstrate the PNI features in KPC mice and expression of Pan-lac, *NSUN2*, *CDCP1*, and *STC1*. *Tuj1* is used as a neuronal marker, while *CK-19* denotes tumor epithelium. Scale bars: H&E and mIF, 200 μm. **(F)** Quantitative assessment of nerve density (above) and nerve count (below) in KPC mice. (n = 15; Chi-square test). **(G)** PNI frequency in KPC mice. (n = 15; Fisher's exact test). **(H)** Severity score of KPC mice. (n = 15; mean ± SD; one-way ANOVA test). *****P < 0.001, ***P < 0.001, ***P < 0.001, ***P < 0.005.

Notably, the lactate-induced enhancement of perineural invasion and upregulation of CDCP1 and STC1 expression were abolished in NSUN2-deficient KPC mice (Figure 6E; Figure S8K-N). Biochemical measurements showed that systemic administration significantly elevated intratumoral lactate concentrations, confirming successful delivery and metabolic impact within the tumor S8O). microenvironment (Figure Consistently, quantification showed a reduced incidence and severity of PNI upon NSUN2 depletion, with lactate again exerting only partial rescue effects (Figure 6F-G). To more rigorously assess neural involvement, tumor sections were stained with the neuronal marker β3-tubulin and independently scored by professional pathologist. PNI severity score = $[(no. of nerves / n0 \times$ 'score 0') + (n1 × 'score 1' / perineural invasion) + (n2 x 'score 2' / endoneural invasion)] / total no. of nerves, where n0, n1 and n2 denote the number of nerves without invasion, with perineural invasion, and with endoneural invasion, respectively [27]. Using this approach, we observed that lactate treatment significantly increased PNI severity, whereas NSUN2 silencing reduced it (Figure 6H). Collectively, these findings demonstrated that NSUN2 lactylation enhances perineural invasion and tumor nerve interactions in pancreatic cancer models.

Association of NSUN2/CDCP1/STC1 with PNI and unfavorable prognosis in PDAC

To investigate the clinical significance of NSUN2 lactylation in PDAC, we assessed their expression via immunohistochemistry (IHC) in tissue samples from 142 PDAC patients, categorized by the presence or absence of severe PNI (Figure 7A). To more precisely assess the clinical relevance of NSUN2, we quantified IHC staining using the H-score method, and the H-score was calculated as: (percentage of weak staining) + $2 \times$ (percentage of moderate staining) + $3 \times$ (percentage of strong staining), yielding a total score of 0-300 [28]. When applied to patient samples, this scoring approach revealed that PNI (+) cases exhibited significantly higher NSUN2 levels than PNI (-) cases (Figure 7B). To further evaluate the diagnostic performance, we conducted ROC curve analysis, which demonstrated that NSUN2 expression

robustly discriminated PNI (+) from PNI (-) tumors, underscoring its predictive value for PNI risk (Figure 7C). Elevated levels of lactylation and NSUN2-related proteins were detected in PNI-high tumors compared with PNI-low cases (Figure 7D). To clarify the potential clinical implications of NSUN2 lactylation, performed co-immunoprecipitation (Co-IP) followed by western blotting on protein extracts from pancreatic tumor tissues. The results revealed that tumors from PNI (+) patients exhibited markedly higher levels of lactylated NSUN2 compared with those from PNI (-) patients (Figure 7E), providing direct clinical evidence that NSUN2 lactylation is associated with perineural invasion. Kaplan-Meier survival analysis demonstrated that a high CDCP1 and STC1 expression was associated with shorter overall survival (OS) and disease-free survival (DFS) In (Figure 7F-I). addition, we performed comprehensive univariate and multivariate Cox regression analyses for both overall survival (OS) and disease-free survival (DFS) in our cohort of 142 PDAC patients. The results demonstrated that PNI was significantly associated with poor prognosis in the univariate model, and importantly, this association remained robust after adjusting for TNM stage and tumor differentiation (Table S4-S5). These findings clearly indicate that the prognostic value of PNI extends beyond established clinical variables and underscore its importance as an independent marker of patient outcome in PDAC. Consistent with these clinical correlations, mechanistic integration of our findings supports a model in which lactylation serves as a pivotal switch controlling NSUN2 stability and downstream oncogenic signaling (Figure 7J). Under low-lactate conditions, NSUN2 undergoes ubiquitination and degradation, leading destabilization and decay of CDCP1 and STC1 transcripts, thereby attenuating PNI. In contrast, high lactate levels promote NSUN2 lactylation, which prevents ubiquitination-mediated degradation, enhances NSUN2 stability, and facilitates selective binding to CDCP1 and STC1 mRNAs. Collectively, our findings suggest that lactylation of NSUN2 may serve as a biomarker for PNI and a potential therapeutic target in PDAC.

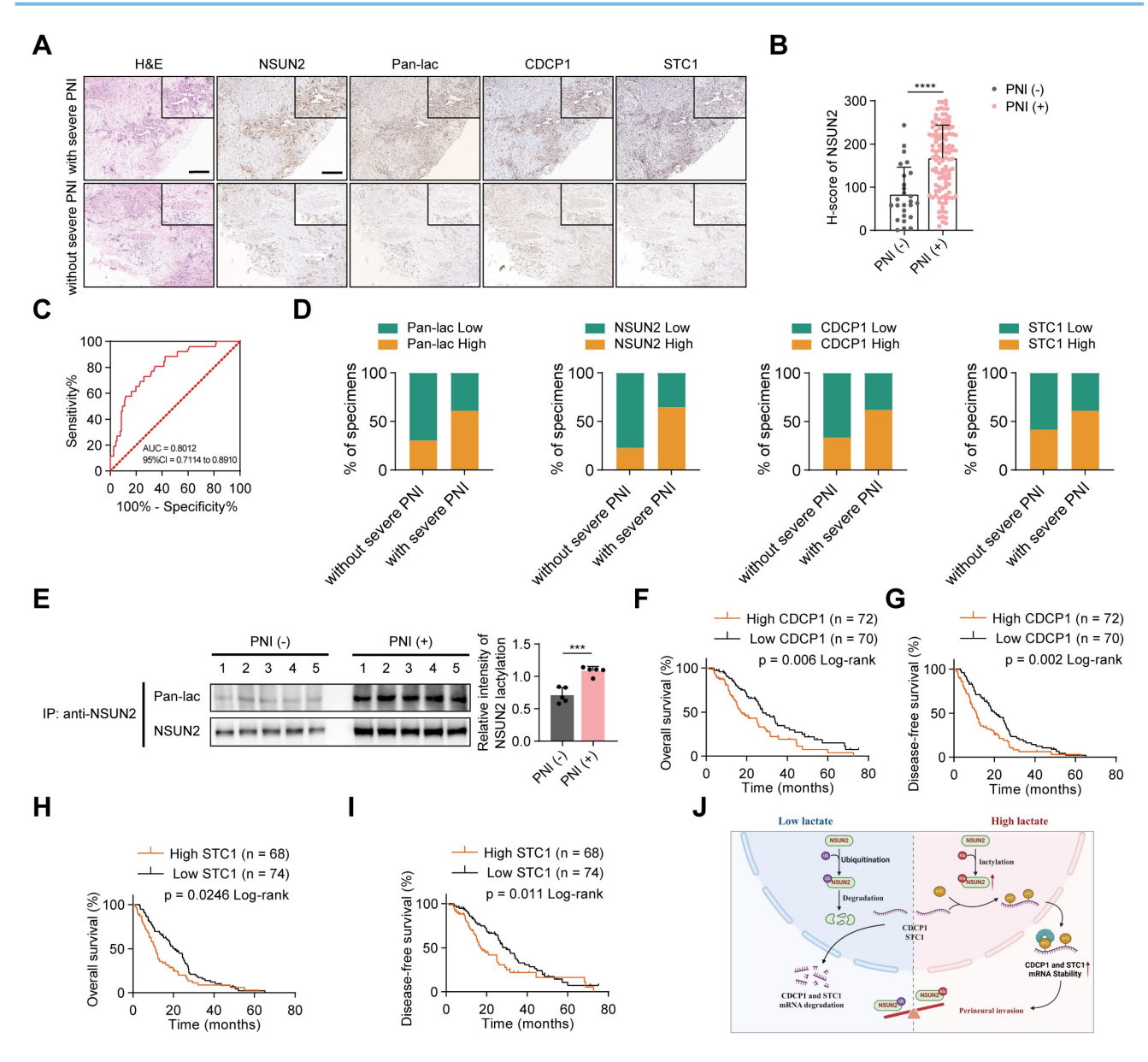


Figure 7. Association of NSUN2/CDCP1/STC1 with PNI and Unfavorable Prognosis in PDAC. (A) H&E and IHC images showing Pan-lac, NSUN2, CDCP1, STC1 expression in PDAC specimens (n = 142). Scale bars, 200 μm. (B) H-score of NSUN2 expression in PDAC patients with or without severe PNI. (C) ROC curve analysis based on NSUN2 H-scores to further evaluate its predictive ability for PNI risk. (D) Proportional distribution of Pan-lac, NSUN2, CDCP1, and STC1 expression in PDAC samples grouped by PNI severity (with or without severe PNI). (E) Lactylation of NSUN2 in PNI(-) or PNI(+) pancreatic cancer tissues (left) and quantification of NSUN2 lactylation intensity normalized to NSUN2 (n = 3; unpaired t test; mean ± SD). (F-I) Kaplan-Meier survival curves showing OS and DFS in the PDAC cohort stratified by CDCP1 (F-G) and STC1 (H-I) level (high vs low). (J) Diagram summarizing the proposed mechanism through which a lactate-enriched tumor microenvironment facilitates pancreatic cancer PNI by upregulating tumor cells NSUN2 lactylation and transcriptionally activating the m5C modification of neural invasion—related genes.

Discussion

While substantial progress has been made in unraveling the complex molecular and signaling interactions involved in PNI, the specific mechanisms by which lactate metabolism drives its progression remain largely unclear. Recent research by Li *et al.* demonstrated that cancer-associated fibroblasts (CAFs) create a lactate-rich microenvironment, which drives histone H3K18 lactylation and consequently promotes the perineural invasion (PNI) of pancreatic

cancer [29]. In addition, Chen *et al.* showed that lactate-induced lactylation of *NSUN2* enhances its binding affinity to ENO1 mRNA and promotes m5C-dependent stabilization, thereby accelerating colorectal cancer progression [7]. These findings collectively highlight the critical roles of both histone and non-histone protein lactylation in promoting tumor progression. Our study demonstrates that patients with severe PNI exhibit markedly elevated lactate and global lactylation levels, which are associated with poor prognosis, identifying *NSUN2* as

mediator in lactylation-induced Mechanistically, lactate accumulation promotes lactylation of NSUN2 at K692, preventing its degradation and enhancing CDCP1 and STC1 mRNA stability through lactvlation modification, inhibition of NSUN2 or its lactvlation significantly reduces neural invasion in a KPC mouse model. Our study reveals that lactylation-induced NSUN2-mediated RNA m5C modification is a crucial driver of PNI in PDAC, highlighting NSUN2 inhibition as a novel and promising therapeutic strategy for addressing this aggressive feature of pancreatic cancer.

Hypoxic tumor cells predominantly rely on glucose for glycolytic energy production, leading to the release of lactic acid, which establishes a lactate gradient that mirrors the tumor's oxygen distribution [30]. Initial studies on metabolites in human cervical cancer [31] and head and neck squamous cell carcinomas [32] suggest a link between the levels of lactate in tumor tissue and the likelihood of metastatic spread. Yu et al. recently reported that reducing lactate levels in the tumor microenvironment can effectively alleviate immunosuppression and boost immune responses, offering a promising approach for pancreatic cancer treatment [33]. Li et al. revealed that enhanced glycolysis, driven by glutamate-induced m6A modification of HK2 mRNA, plays a crucial role in promoting PNI in PDAC, highlighting the significant impact of metabolic regulation on PNI [34]. Nevertheless, the correlation between lactate levels and the extent of PNI in PDAC has not been elucidated. Our study is the first to establish this connection, suggesting a critical role for lactate in modulating PNI, thereby unveiling a previously uncharted dimension of tumor pathophysiology. Lactylation, a key and widespread post-translational protein modification, has recently been shown to be highly expressed in PDAC and is associated with poor patient prognosis [35]. Wang et al. recently PYCR1 regulates demonstrated that lactate metabolism via histone lactylation to modulate IRS1 expression, thereby promoting liver cancer metastasis [36]. Our research found that patients with advanced PNI show significantly elevated pan-lactylation, highlighting mechanism crucial metabolic-epigenetic coupling within PNI microenvironment in PDAC.

Growing evidence has established a link between aberrant m5C modifications and a range of diseases, including cancers, heart disease, neurodegenerative disorders, and chronic inflammation [8,9,37-41]. We recently found that CAFs enhance pancreatic cancer cell PNI by modulating the function of YBX1, an m5C reader,

enabling it to selectively recognize and stabilize PNI-related mRNAs [10]. Notably, we also observed a correlation between increased PNI and elevated m5C levels, though the underlying mechanism remains to be explored. Recent studies have highlighted the role of lactate in regulating RNA modifications, particularly through lactylation-driven mechanisms [42]. Xiong et al. demonstrated that lactate induces the expression and activity of the RNA methyltransferase METTL3, enhancing immunosuppressive functions of tumor-infiltrating myeloid cells and promoting immune evasion in tumors [43]. Similarly, Yu et al. showed that histone lactylation accelerates tumorigenesis by activating the m6A reader YTHDF2 [44], while Gu et al. further demonstrated that lactylation activates ALKBH3, modulating m1A modification, thereby highlighting the close interplay between lactylation and RNA methylation in tumor progression [45]. In our study, we for the first time connected lactylation with m5C RNA modification, uncovering a novel regulatory axis in tumor metastasis and advancing the understanding of how metabolic and epigenetic modifications interact.

A previous study reported that the expression of the m5C methyltransferase NOP2/Sun RNA methyltransferase family member 2 (NSUN2) was aberrantly elevated in pancreatic tumors [46]. The role of lactylation in regulating NSUN2 expression in pancreatic cancer remains unclear. Recent studies have highlighted the role of NSUN2 upregulation and its RNA m5C modification in Cr(VI)-induced lung tumor progression, where NSUN2 expression is transcriptionally activated by EP300 via histone acetylation (H3K27ac) [47]. Additionally, in colorectal cancer cells, lactate accumulation promotes NSUN2 transcription through histone H3K18 lactylation, which in turn induces lactylation of NSUN2 at Lys356, crucial for binding to specific RNAs and facilitating the m5C modification of ENO1 mRNA [7]. In contrast to previous studies, our research found that lactate does not upregulate the mRNA expression of NSUN2 in pancreatic cancer cells. However, lactylation of NSUN2 inhibits its ubiquitination and degradation by disrupting its interaction with STUB1, thereby enhancing its stability in the presence of lactate. This suggests that lactylation modification may exert heterogeneous regulatory effects across different diseases and highlights the functional diversity of lactylation in modulating key protein modifications. Recent studies have illuminated the complex post-translational regulation of NSUN2, highlighting its diverse functional modifications. Zhang et al. identified NSUN2 as a target of the E3 ubiquitin ligase STUB1, which mediates its ubiquitination and

degradation during hepatocyte ferroptosis [19]. Additionally, SUMO-2/3 has been shown to stabilize NSUN2 and facilitate its nuclear transport in gastric cancer [48], while glucose-induced oligomerization and activation of NSUN2 promote TREX2 expression, suppressing cGAS/STING activation to regulate oncogenic activity in cancer cells [49]. We elucidated that lactylation at NSUN2-K692 inhibits ubiquitination and promotes PNI in pancreatic cancer. RIP-seq shows that NSUN2 binds chiefly within coding exons, with fewer but notable peaks in 3' UTRs and very few in 5' UTRs. Lactate slightly amplifies the 3' UTR fraction without changing this hierarchy. This distribution pattern is consistent with the RIP-seq results of NSUN2 reported by Wenlan Yang et al., which showed that in Th17 cells, NSUN2-binding peaks were primarily located in the CDS region of mRNA transcripts, followed by the 3' UTR [50]. Through comprehensive analysis of NSUN2 RIP-Seq and RNA-Seq under L-lactate treatment, we identified PNI-associated genes, CDCP1 and STC1, as key targets. Further MeRIP-PCR analysis revealed that NSUN2 primarily enhances the m5C modification on CDCP1 and STC1, thereby stabilizing their mRNA. While Chen et al. shown that lactate binds to NSUN2-K356 to facilitate the capture m5C-modified RNAs in colorectal cancer [7], whether lactylation at NSUN2-K692 similarly aids in the m5C modification of CDCP1 and STC1 remains an intriguing avenue for further investigation. Our study unveils the novel role of NSUN2 lactylation at K692 in regulating m5C modifications of CDCP1 and STC1, emphasizing the distinctive role of lactylation in modulating PNI and highlighting its potential as a therapeutic target.

While previous studies have demonstrated that both histone and non-histone lactylation contribute to pancreatic cancer invasion and metastasis [17,51], and that lactylation can regulate tumor progression by influencing methylation modifications [52], our study presents a novel perspective by uncovering the cooperative role of lactylation and m5C methylation in perineural invasion (PNI) of pancreatic cancer. Specifically, we reveal that metabolic activation leads to intracellular lactate accumulation, which selectively induces lactylation of NSUN2, the critical m5C writer enzyme. This modification enhances NSUN2 protein stability, thereby increasing m5C modificationmediated stabilization of key PNI-related genes. The resulting upregulation of their post-transcriptional expression creates a previously unrecognized regulatory axis between protein lactylation and RNA methylation, which plays a crucial role in PNI progression. By elucidating this precise regulatory interplay between protein and RNA modifications,

our findings expand the understanding of metabolic-epigenetic crosstalk in pancreatic cancer and offer novel insights into targeted therapeutic strategies aimed at disrupting specific modification pathways. This study provides a foundation for future research into metabolic reprogramming-driven epigenetic regulation in aggressive tumor behaviors, including PNI.

In conclusion, our study is the first to uncover the cooperative role of epigenetic modifications in governing PNI progression in pancreatic cancer. Our findings demonstrate that major PNI-related genes are tightly regulated through *NSUN2*-mediated m5C modification, which is driven by lactylation of *NSUN2*. Our findings highlight the potential of targeting *NSUN2* lactylation and inhibiting m5C modification as promising strategies to prevent PNI and improve therapeutic outcomes in pancreatic cancer.

Supplementary Material

Supplementary figures and tables. https://www.thno.org/v16p1782s1.pdf

Acknowledgements

This work was financially supported by the National Natural Science Foundation of China (grant numbers 82372859 and 82573586 to S.Z., 82573083 and 82203691 to C.H., 82572511 to X.W., KY012023453, 82072639 and 82372858 to R.C., 82403081 to H.C., and 4130023082 to Z.L. and M.X.), the Natural Science Foundation of Guangdong Province (grant number 2024A1515013216 to C.H.), the Special Fund of 'Dengfeng Plan' of Guangdong Provincial People's Hospital, China (grant numbers KJ012019509 and DFJH2020027 to R.C.), and the National Key Clinical Specialty Construction Project (2021–2024, grant number 2022YW030009 to R.C.).

Author contributions

S.Z. and R.C. conceived and supervised the overall project and acquired funding. X.W. study design assisted in and contributed to manuscript writing. T.H. carried out the majority of experiments, performed data analysis, and wrote the initial draft. C.H., H.C., and H.J. were responsible for primary cells isolation, cell culture, plasmid construction, establishment of mouse models, immunoprecipitation, and Western blotting. Q.T., R.H., and T.L. collected patient information and PDAC tissue samples. H.J., Z.L. and M.X. conducted RNA sequencing and ubiquitination analyses. Y.Y. and Y.J. clinical data collection supported the interpretation.

Data availability

The RNA-seq datasets generated and analyzed during this study have been deposited in the Gene Expression Omnibus (GEO) under accession number GSE299600, and the RIP-seq datasets generated and analyzed during this study have been deposited in the GEO under accession number GSE299599. The raw and processed data will be made available upon publication. Other relevant materials are available from the corresponding author upon reasonable request.

Competing Interests

The authors have declared that no competing interest exists.

References

- Winkler F, Venkatesh HS, Amit M, Batchelor T, Demir IE, Deneen B, et al. Cancer neuroscience: State of the field, emerging directions. Cell. 2023; 186(8): 1689-1707.
- Bapat AA, Hostetter G, Von Hoff DD, Han H. Perineural invasion and associated pain in pancreatic cancer. Nat Rev Cancer. 2011; 11(10): 695-707.
- Demir IE, Boldis A, Pfitzinger PL, Teller S, Brunner E, Klose N, et al. Investigation of schwann cells at neoplastic cell sites before the onset of cancer invasion. J Natl Cancer Inst. 2014; 106(8):
- Sinha S, Fu YY, Grimont A, Ketcham M, Lafaro K, Saglimbeni JA, et al. Panin neuroendocrine cells promote tumorigenesis via neuronal cross-talk. Cancer Res. 2017; 77(8): 1868-1879.
- Lin Q, Zheng S, Yu X, Chen M, Zhou Y, Zhou Q, et al. Standard pancreatoduodenectomy versus extended pancreatoduodenectomy with modified retroperitoneal nerve resection in patients with pancreatic head cancer: A multicenter randomized controlled trial. Cancer Commun (Lond). 2023; 43(2): 257-275.
- Zou Z, Dou X, Li Y, Zhang Z, Wang J, Gao B, et al. Rna m(5)c oxidation by tet2 regulates chromatin state and leukaemogenesis. Nature. 2024; 634(8035): 986-994.
- Chen B, Deng Y, Hong Y, Fan L, Zhai X, Hu H, et al. Metabolic recoding of NSUN2-mediated m(5)c modification promotes the progression of colorectal cancer via the NSUN2/ybx1/m(5)c-eno1 positive feedback loop. Adv Sci (Weinh). 2024; 11(28): e2309840.
- Chen X, Li A, Sun BF, Yang Y, Han YN, Yuan X, et al. 5-methylcytosine promotes pathogenesis of bladder cancer through stabilizing mrnas. Nat Cell Biol. 2019; 21(8): 978-990.
- Su J, Wu G, Ye Y, Zhang J, Zeng L, Huang X, et al. NSUN2-mediated rna 5-methylcytosine promotes esophageal squamous cell carcinoma progression via lin28b-dependent grb2 mrna stabilization. Oncogene. 2021; 40(39): 5814-5828.
- Zheng S, Hu C, Lin Q, Li T, Li G, Tian Q, et al. Extracellular vesicle-packaged piat from cancer-associated fibroblasts drives neural remodeling by mediating m5c modification in pancreatic cancer mouse models. Sci Transl Med. 2024; 16(756): eadi0178.
- Kumagai S, Koyama S, Itahashi K, Tanegashima T, Lin YT, Togashi Y, et al. Lactic acid promotes pd-1 expression in regulatory t cells in highly glycolytic tumor microenvironments. Cancer Cell. 2022; 40(2): 201-218 e9.
- 12. Chen J, Zhu Y, Wu C, Shi J. Engineering lactate-modulating nanomedicines for cancer therapy. Chem Soc Rev. 2023; 52(3): 973-1000.
- Certo M, Tsai CH, Pucino V, Ho PC, Mauro C. Lactate modulation of immune responses in inflammatory versus tumour microenvironments. Nat Rev Immunol. 2021; 21(3): 151-161.
- Li X, Yang Y, Zhang B, Lin X, Fu X, An Y, et al. Lactate metabolism in human health and disease. Signal Transduct Target Ther. 2022; 7(1): 305.
- Liberti MV, Locasale JW. Histone lactylation: A new role for glucose metabolism. Trends Biochem Sci. 2020; 45(3): 179-182.
- De Leo A, Ugolini A, Yu X, Scirocchi F, Scocozza D, Peixoto B, et al. Glucose-driven histone lactylation promotes the immunosuppressive activity of monocyte-derived macrophages in glioblastoma. Immunity. 2024; 57(5): 1105-1123 e8.
- Li F, Si W, Xia L, Yin D, Wei T, Tao M, et al. Positive feedback regulation between glycolysis and histone lactylation drives oncogenesis in pancreatic ductal adenocarcinoma. Mol Cancer. 2024; 23(1): 90.
- Cui L, Ma R, Cai J, Guo C, Chen Z, Yao L, et al. Rna modifications: Importance in immune cell biology and related diseases. Signal Transduct Target Ther. 2022; 7(1): 334.

- Zhang X, Zhang Y, Li R, Li Y, Wang Q, Wang Y, et al. STUB1-mediated ubiquitination and degradation of NSUN2 promotes hepatocyte ferroptosis by decreasing m(5)c methylation of gpx4 mrna. Cell Rep. 2024; 43(11): 114885.
- Yang W, Liu L, Li C, Luo N, Chen R, Li L, et al. Trim52 plays an oncogenic role in ovarian cancer associated with nf-kb pathway. Cell Death Dis. 2018; 9(9): 908
- Qin S, Guo Q, Liu Y, Zhang X, Huang P, Yu H, et al. A novel tgfbeta/tgilr axis mediates crosstalk between cancer-associated fibroblasts and tumor cells to drive gastric cancer progression. Cell Death Dis. 2024; 15(5): 368.
- Liu A, Li Y, Lu S, Cai C, Zou F, Meng X. Stanniocalcin 1 promotes lung metastasis of breast cancer by enhancing egfr-erk-s100a4 signaling. Cell Death Dis. 2023; 14(7): 395.
- Khan T, Kryza T, Lyons NJ, He Y, Hooper JD. The CDCP1 signaling hub: A target for cancer detection and therapeutic intervention. Cancer Res. 2021; 81(9): 2259-2269.
- Xu L, Hu H, Zheng LS, Wang MY, Mei Y, Peng LX, et al. Etv4 is a theranostic target in clear cell renal cell carcinoma that promotes metastasis by activating the pro-metastatic gene FOSL1 in a pi3k-akt dependent manner. Cancer Lett. 2020: 487-74-89
- Zhang D, Zhang JW, Xu H, Chen X, Gao Y, Jiang HG, et al. Therapy-induced senescent tumor cell-derived extracellular vesicles promote colorectal cancer progression through Serpine1-mediated nf- κ b p65 nuclear translocation. Mol Cancer. 2024; 23(1): 70.
- 26. Mayr C. What are 3' utrs doing? Cold Spring Harb Perspect Biol. 2019; 11(10):
- 27. Wang X, Istvanffy R, Ye L, Teller S, Laschinger M, Diakopoulos KN, et al. Phenotype screens of murine pancreatic cancer identify a tgf-alpha-ccl2-paxillin axis driving human-like neural invasion. J Clin Invest. 2023; 133(21):
- Xu J, Yang X, Deng Q, Yang C, Wang D, Jiang G, et al. Tem8 marks neovasculogenic tumor-initiating cells in triple-negative breast cancer. Nat Commun. 2021; 12(1): 4413.
- Li T, Hu C, Huang T, Zhou Y, Tian Q, Chen H, et al. Cancer-associated fibroblasts foster a high-lactate microenvironment to drive perineural invasion in pancreatic cancer. Cancer Res. 2025; 85(12): 2199-2217.
- Sonveaux P, Vegran F, Schroeder T, Wergin MC, Verrax J, Rabbani ZN, et al. Targeting lactate-fueled respiration selectively kills hypoxic tumor cells in mice. J Clin Invest. 2008; 118(12): 3930-42.
- Schwickert G, Walenta S, Sundfor K, Rofstad EK, Mueller-Klieser W. Correlation of high lactate levels in human cervical cancer with incidence of metastasis. Cancer Res. 1995; 55(21): 4757-9.
- Walenta S, Salameh A, Lyng H, Evensen JF, Mitze M, Rofstad EK, et al. Correlation of high lactate levels in head and neck tumors with incidence of metastasis. Am J Pathol. 1997; 150(2): 409-15.
- Yu N, Zhou J, Ding M, Li M, Peng S, Li J. Sono-triggered cascade lactate depletion by semiconducting polymer nanoreactors for cuproptosis-immunotherapy of pancreatic cancer. Angew Chem Int Ed Engl. 2024; 63(30): e202405639.
- Li F, He C, Yao H, Zhao Y, Ye X, Zhou S, et al. Glutamate from nerve cells promotes perineural invasion in pancreatic cancer by regulating tumor glycolysis through hk2 mrna-m6a modification. Pharmacol Res. 2023; 187: 106555.
- Huang H, Wang S, Xia H, Zhao X, Chen K, Jin G, et al. Lactate enhances nmnat1 lactylation to sustain nuclear nad(+) salvage pathway and promote survival of pancreatic adenocarcinoma cells under glucose-deprived conditions. Cancer Lett. 2024: 588: 216806.
- Wang H, Xu M, Zhang T, Pan J, Li C, Pan B, et al. Pycr1 promotes liver cancer cell growth and metastasis by regulating irs1 expression through lactylation modification. Clin Transl Med. 2024; 14(10): e70045.
- Balachander K, Priyadharsini JV, Roy A, Paramasivam A. Emerging role of rna m5c modification in cardiovascular diseases. J Cardiovasc Transl Res. 2023; 16(3): 598-605.
- Blanco S, Dietmann S, Flores JV, Hussain S, Kutter C, Humphreys P, et al. Aberrant methylation of trnas links cellular stress to neuro-developmental disorders. Embo j. 2014; 33(18): 2020-39.
- Luo Y, Feng J, Xu Q, Wang W, Wang X. NSUN2 deficiency protects endothelium from inflammation via mrna methylation of icam-1. Circ Res. 2016; 118(6): 944-56.
- Rajpurohit T, Bhattacharya S. Moving towards dawn: Kras signaling and treatment in pancreatic ductal adenocarcinoma. Curr Mol Pharmacol. 2022; 15(7): 904-928.
- Magouliotis DE, Sakellaridis N, Dimas K, Tasiopoulou VS, Svokos KA, Svokos AA, et al. In silico transcriptomic analysis of the chloride intracellular channels (clic) interactome identifies a molecular panel of seven prognostic markers in patients with pancreatic ductal adenocarcinoma. Curr Genomics. 2020; 21(2): 119-127.
- 42. Yang Z, Zheng Y, Gao Q. Lysine lactylation in the regulation of tumor biology. Trends Endocrinol Metab. 2024; 35(8): 720-731.
- Xiong J, He J, Zhu J, Pan J, Liao W, Ye H, et al. Lactylation-driven mettl3-mediated rna m(6)a modification promotes immunosuppression of tumor-infiltrating myeloid cells. Mol Cell. 2022; 82(9): 1660-1677 e10.
- Yu J, Chai P, Xie M, Ge S, Ruan J, Fan X, et al. Histone lactylation drives oncogenesis by facilitating m(6)a reader protein ythdf2 expression in ocular melanoma. Genome Biol. 2021; 22(1): 85.
- 45. Gu X, Zhuang A, Yu J, Yang L, Ge S, Ruan J, et al. Histone lactylation-boosted alkbh3 potentiates tumor progression and diminished promyelocytic

- leukemia protein nuclear condensates by m1a demethylation of sp100a. Nucleic Acids Res. 2024; 52(5): 2273-2289.
- Okamoto M, Hirata S, Sato S, Koga S, Fujii M, Qi G, et al. Frequent increased gene copy number and high protein expression of trna (cytosine-5-)-methyltransferase (NSUN2) in human cancers. DNA Cell Biol. 2012; 31(5): 660-71.
- 47. Zhang RK, Li Y, Sun FL, Zhou ZH, Xie YX, Liu WJ, et al. Rna methyltransferase NSUN2-mediated m5c methylation promotes cr(vi)-induced malignant transformation and lung cancer by accelerating metabolism reprogramming. Environ Int. 2024; 192: 109055.
- Hu Y, Chen C, Tong X, Chen S, Hu X, Pan B, et al. NSUN2 modified by sumo-2/3 promotes gastric cancer progression and regulates mrna m5c methylation. Cell Death Dis. 2021; 12(9): 842.
- Chen T, Xu ZG, Luo J, Manne RK, Wang Z, Hsu CC, et al. NSUN2 is a glucose sensor suppressing cgas/sting to maintain tumorigenesis and immunotherapy resistance. Cell Metab. 2023; 35(10): 1782-1798 e8.
- 50. Yang WL, Qiu W, Zhang T, Xu K, Gu ZJ, Zhou Y, et al. NSUN2 coupling with ror γ t shapes the fate of th17 cells and promotes colitis. Nat Commun. 2023; 14(1): 863
- Chen M, Cen K, Song Y, Zhang X, Liou YC, Liu P, et al. Nusap1-LDHA-glycolysis-lactate feedforward loop promotes warburg effect and metastasis in pancreatic ductal adenocarcinoma. Cancer Lett. 2023; 567: 216285.
- Sun L, Zhang Y, Yang B, Sun S, Zhang P, Luo Z, et al. Lactylation of mettl16 promotes cuproptosis via m(6)a-modification on fdx1 mrna in gastric cancer. Nat Commun. 2023; 14(1): 6523.